Mucoricin is a Ricin-Like Toxin that is Critical for the Pathogenesis of Mucormycosis

Sameh S. M. Soliman,[1,2‡] Clara Baldin,[1,3‡] Yiyou Gu,[1‡] Shakti Singh,[1‡] Teclegiorgis Gebremariam,[1] Marc Swidergall,[1,4] Abdullah Alqarihi,[1] Eman G. Youssef,[1,5] Sondus Alkhazraji,[1] Antonis Pikoulas,[6] Christina Perske,[7] Vivek Venkataramani,[7,8] Abigail Rich,[9] Vincent M. Bruno,[10] Julie Dunning Hotopp,[10] Nicolas J. Mantis,[11] John E. Edwards, Jr.[1,4] Scott G. Filler,[1,4] Georgios Chamilos,[6] Ellen S. Vitetta,[9] Ashraf S. Ibrahim[1,4*]

[1]Division of Infectious Diseases, The Lundquist Institute for Biomedical Innovation at Harbor-University of California at Los Angeles (UCLA) Medical Center , Torrance, CA, U.S.A.; [2] College of Pharmacy and Research Institute for Medical and Health Sciences, University of Sharjah, P.O. Box 27272, Sharjah, United Arab Emirates; [3]Department of Biological Chemistry, Medical University of Innsbruck, Innsbruck, Austria; [4]David Geffen School of Medicine at UCLA, Los Angeles, Ca, U.S.A; [5]Department of Biotechnology and Life Sciences, Faculty of Postgraduate Studies for Advanced Sciences, Beni-Suef University, Beni-Suef, Egypt; [6]Department of Medicine, University of Crete, Foundation for Research and Technology, 71300 Heraklion, Crete, Greece; [7]Department of Pathology, University Medicine Göttingen, Göttingen, Germany; [8]Department of Hematology and Medical Oncology, University Medicine Göttingen, Göttingen, Germany; [9]Departments of Immunology and Microbiology, UT Southwestern Medical Center, Dallas, Tx, U.S.A; [10]Department of Microbiology and Immunology, University of Maryland School of Medicine, Baltimore, MD, U.S.A [11] New York State Department of Health, Wadsworth Center**,** Albany, NY, U.S.A.

[‡]Equal contribution

***Corresponding Author: Ashraf S. Ibrahim**

24 Division of Infectious Diseases (MRL), 1124 W. Carson St., Torrance, CA 90502.

25 Tel: (310) 222-6424, Fax: (310) 782-2016, e-mail; ibrahim@lundquist.org

26 Short title: Mucormycosis involves a ricin-like toxin

27

Abstract

Fungi of the order Mucorales cause mucormycosis, a lethal infection with an incompletely understood pathogenesis. We now demonstrate that Mucorales fungi produce a toxin that plays a central role in virulence. Polyclonal antibodies against this toxin inhibit its ability to damage human cells *in vitro,* and prevent hypovolemic shock, organ necrosis, and death in mice with mucormycosis. RNAi inhibition of the toxin in *Rhizopus delemar,* compromises the ability of the fungus to damage host cells and attenuates virulence in mice. This 17 kDa toxin has structural and functional features of the plant toxin, ricin, including the ability to inhibit protein synthesis by its N-glycosylase activity, the existence of a motif that mediates vascular leak, and a lectin sequence. Antibodies against the toxin inhibit *R. delemar*- or toxin-mediated vascular permeability *in vitro* and cross-react with ricin. A monoclonal anti-ricin B chain antibody binds to the toxin and also inhibits its ability to cause vascular permeability. Therefore, we propose the name "mucoricin" for this toxin. Not only is mucoricin important in the pathogenesis of mucormycosis but our data suggest that a ricin-like toxin is produced by organisms beyond the plant and bacterial kingdoms. Importantly, mucoricin should be a promising therapeutic target.

Keywords: Mucormycosis, Toxins, Ricin, *Rhizopus*, Virulence, Pathogenesis, Mucoricin

Word count: 200

Mucormycosis is a lethal fungal infection that usually afflicts immunocompromised hosts such as diabetics in ketoacidosis (DKA), neutropenic patients, patients undergoing hematopoietic cell or solid organ transplant, or patients receiving high-dose corticosteroids[1-6]. Immunocompetent patients with severe trauma are also at risk of contracting mucormycosis by direct inoculation of open wounds[7,8]. The overall mortality rate of mucormycosis is >40% and it approaches 100% in patients with disseminated disease, persistent neutropenia, or brain infection[1-6]. The two most common forms of the disease are rhino-orbital/cerebral and pulmonary mucormycosis. In both forms of the disease, infection is initiated by the inhalation of spores that germinate in the host to form hyphae, which are capable of invading host tissues while avoiding phagocytic killing[6,9].

A characteristic feature of mucormycosis is the propensity of Mucorales to invade blood vessels, resulting in thrombosis and subsequent tissue necrosis[6]. The massive tissue necrosis associated with mucormycosis compromises the delivery of antifungal drugs to infected foci, thereby necessitating radical surgical intervention to improve the outcome of therapy. We have previously determined that Mucorales fungi invade human umbilical vein endothelial cells (HUVECs) by expressing the fungal invasin, CotH3, which interacts with the 78kDa host receptor, glucose regulated protein (GRP78). The interaction between CotH3 and GRP78 induces the endothelial cells to endocytose the fungi[10-12]. However, the mechanisms by which Mucorales damage host cells and cause necrosis are unknown.

While studying the capacity of *Rhizopus delemar,* the most common cause of mucormycosis, to damage HUVECs, we observed that killed hyphae of this organism and other Mucorales caused considerable damage to host cells[13]. This experimental finding and the clinical

observation of the extensive tissue necrosis observed in patients with mucormycosis led us to speculate that a fungal-derived toxin may be involved in the pathogenesis of this disease.

Here, we identify and characterize a hyphal-associated and secreted/shed toxin produced by Mucorales. This toxin damages host cells *in vitro* by inhibiting protein synthesis. The toxin is required for the pathogenesis of mucormycosis in mice, where it induces inflammation, hemorrhage and tissue damage resulting in apoptosis and necrosis. Suppression of toxin production in *R. delemar* by RNAi attenuates virulence in DKA mice, and polyclonal anti-toxin antibodies (IgG anti-toxin) protect mice from mucormycosis by reducing tissue inflammation and damage. Thus, the toxin is a key virulence factor of Mucorales fungi and a promising therapeutic target. Because this toxin shares structural and functional features with ricin produced by the castor bean plant, *Ricinus communis*[14], we named it "mucoricin".

Results

Mucorales damage host cells by a hyphal-associated toxin

We previously observed that *R. delemar* causes significant damage to HUVECs within 8 h of infection[11]. This organism also damages the A549 alveolar epithelial cell line and primary alveolar epithelial cells, but only after 30 h of incubation (**Extended Data Fig. 1a**). *R. delemar*-mediated damage to both HUVECs and alveolar epithelial cells is associated with the formation of extensive hyphae, suggesting that the hyphal form of this organism produces a factor(s) that damage host cells[13]. To investigate whether viability is required for *R. delemar* hyphae to damage host cells, we compared the extent of damage to A549 cells caused by live and heat-killed hyphae. We found that while heat-killed hyphae caused less damage to these cells than live hyphae, the extent of host cell damage was still significant (**Extended Data Fig. 1b)**. These

finding suggested that a hyphal-associated heat-stable toxin may be partially responsible for host cell damage. To explore this hypothesis, we compared the ability of aqueous extracts from dead *R. delemar* spores and/or hyphae to damage host cells. Extracts from either hyphae alone or from a mixture of spores and hyphae damaged A549 cells, whereas an extract from spores alone caused no detectable damage (**Extended Data Fig. 1c**). We also found that killed cells and pelleted hyphal debris from four different Mucorales fungi, but not the yeast *Candida albicans,* caused significant damage to HUVECs (**Extended Data Fig. 1d**). Collectively, these results suggest that Mucorales produce a hyphal-associated toxin that damages mammalian cells.

Purification and activity of the toxin

To purify the hyphal-associated toxin, *R. delemar* spores were grown in a liquid medium for 4-7 days to generate a hyphal mat. The mat was ground in liquid nitrogen and extracted with sterile water, concentrated and analyzed by size exclusion chromatography[15]. When the different fractions were analyzed for their ability to damage A549 cells, activity was found in the fractions with molecular masses of 10-30 kDa (**Extended Data Fig. 2a**). The concentrated water extract was then subjected to three dimensional chromatographic fractionations yielding a fraction that caused significant damage to A549 cells (**Extended Data Fig. 2b-g**). This fraction was further subjected to high-performance liquid chromatography (HPLC), using hydrophobic interaction chromatography (HIC). The purified sample was trypsinized and sequenced using LC-MS/MS, which identified a 17 kDa protein (RO3G_06568).

The ORF encoding the 17 kDa protein is widely present in other Mucorales that we and others previously sequenced[16-19] and that are reported to cause disease in humans (*Mucor, Cunninghamella, Lichtheimia*), animals (*Mortierella*), or plants (*Choanephora cucurbitarum*).

Orthologues were also found in the arbuscular mycorrhizal fungus *Rhizophagus* species, and bacterial genera of *Streptomyces* and *Paenibacillus* (**Supplementary Table 1**). Since orthologues were detected in other Mucorales known to cause mucormycosis, we examined the ability of unfractionated hyphal extracts from various Mucorales fungi to damage A549 cells relative to that induced by hyphal extracts from the *R. delemar* 99-880 reference strain. Hyphal extracts from *R. oryzae*, another strain of *R. delemar*, *Lichtheimia corymbifera*, and *Cunninghamella bertholletiae* all caused significant damage to A549 cells (**Extended Data Fig. 1e**).

We expressed the 17 kDa putative toxin gene in *S. cerevisiae* and used the purified recombinant toxin to raise polyclonal anti-toxin antibodies in rabbits. Although the IgG fraction of the antisera (IgG anti-toxin) had no effect on the growth or germination of *R. delemar in vitro* (**Extended Data Fig. 3**), it resulted in ~50%-70% inhibition of the damage to A549 cells caused by heat-killed hyphae of several Mucorales (**Extended Data Fig. 1f**). From these findings we concluded that the putative toxin is responsible for host cell damage caused by most, if not all, members of the Mucorales fungi.

We also used qRT-PCR to study the expression of this ORF in *R. delemar.* In accordance with data showing a lack of toxin activity in spores (**Extended Data Fig. 1c**), there was minimal expression of this gene during the first 3 h of incubation (prior to germination[13]). Expression of this gene began to increase when the spores germinated at 4 h[13], peaked by 5 h, and plateaued for at least 16 h of hyphal formation (**Extended Data Fig. 4a**). Protein expression in germlings and hyphae, but not spores, was confirmed by immunostaining using the IgG anti-toxin (**Extended Data Fig. 4b**). The expression of the putative toxin gene was high in hyphae growing under aerated conditions, but not in hyphae grown in the absence of aeration (**Extended Data Fig. 4c).** In addition, RNA expression was 5-10-fold higher following 2-5 h of co-culture with A549

alveolar epithelial cells as compared to co-culture with HUVECs or human erythrocytes. (**Extended Data Fig. 4d**).

The toxin is capable of damaging host cells *in vitro* and *in vivo*

We compared the ability of the purified toxin to damage primary lung epithelial cells, A549 alveolar epithelial cells, and HUVECs. After 1 h, the toxin caused significant damage to all the host cells and especially to HUVECs (**Fig. 1a**). After 3 h, there was almost 100% damage to all host cells. We also compared the ability of the purified toxin *vs.* the recombinant toxin to damage A549 cells. Both caused significant damage (**Fig. 1b**). Therefore, the purified and the recombinant protein act similarly and in a time dependent manner in damaging A549 cells.

We next tested the activity of the toxin *in vivo*. Toxin purified from *R. delemar* was injected intravenously into mice every other day for a total of three doses and the mice were monitored for behavioral changes, weight loss, and survival. Within 10-30 minutes after the injection of 0.1 mg/ml (5.9 μM) purified toxin, we observed behavior highly suggestive of sudden circulatory hypovolemic shock, including rapid and shallow breathing, weakness, and cold skin. The mice lost >25% of their original body weight (**Fig. 1c**); most eventually died. These events were similar to those observed in mice infected with live *R. delemar* spores (**Fig. 1d**). Finally, histopathology of organs collected from the mice showed pathological changes that included necrosis, hemorrhage, and infiltration of the pulmonary interstitium by macrophages in the lungs. Liver changes included necrosis, clusters of mononuclear cells and the presence of megakaryocytes in the organs, polymorphonuclear cell (PMN) infiltration and tissue calcification indicative of uncontrolled inflammation, hemorrhage and necrosis (**Fig. 1e**). These data suggest

that the toxin is sufficient to cause clinical symptoms often associated with disseminated mucormycosis.

RNAi knockdown and antibody-mediated neutralization of the toxin reduced the virulence of *R. delemar in vitro* and *in vivo*

To further confirm the role of this toxin in the pathogenesis of mucormycosis, we used RNAi[20] to down regulate the gene expression of the toxin. The extent of down regulation of the toxin was measured by qRT-PCR using toxin specific primers and by Western blotting or immunostaining of *R. delemar* with the IgG anti-toxin. This IgG anti-toxin specifically recognized the toxin by ELISA and Western blotting. RNAi knockdown of the toxin caused ~90% inhibition in gene expression (**Extended Data Fig. 5a**). Furthermore, RNAi knockdown resulted in >80% reduction in protein expression (**Extended Data Fig. 5b**) and negligible staining of toxin-RNAi *R. delemar* germlings compared to germlings of a control strain that have been transformed with an empty plasmid (**Extended Data Fig. 5c**). In accord with the lack of an effect by the IgG anti-toxin on the growth and germination of *R. delemar*, the RNAi knockdown of the toxin had no effect on fungal germination or growth (**Extended Data Fig. 6**).

We next assessed the effect of downregulation of toxin expression on the ability of *R. delemar* to damage A549 alveolar epithelial cells. *R. delemar* with RNAi targeting of the toxin gene induced ~40% reduction in epithelial cell damage relative to either the wild-type strain or *R. delemar* transformed with the empty plasmid (**Fig. 2a**). Similarly, the IgG anti-toxin protected alveolar epithelial cells from wild-type *R. delemar*-induced injury by ~40%, *in vitro* whereas normal rabbit IgG did not (**Fig. 2b**).

Finally, we evaluated the effects of RNAi inhibition of toxin production on the virulence of *R. delemar* in our model of pulmonary mucormycosis[21]. DKA mice infected with *R. delemar* harboring the empty plasmid had a median survival time of 6 days and 90% mortality by day 21 post-intratracheal infection, whereas mice infected with the toxin-attenuated expression strain had a median survival time of 21 days and mortality of 30% (**Fig. 2c**). Surviving mice had no residual fungal colonies in their lungs when the experiment was terminated on day 21. Inhibition of toxin production appeared to have minimal effects on the early stages of infection because after 4 days of infection, the fungal burden of the lungs and brains (the primary and secondary target organs, respectively[21]) of mice infected with *R. delemar* toxin-attenuated strain and *R. delemar* harboring the empty plasmid were similar (**Extended Data Fig. 7a**). Reduced virulence without affecting tissue fungal burden has been reported for non-neutropenic mice infected with an *Aspergillus fumigatus* null mutant that does not produce the Asp f1 ribotoxin[22], representing a classical feature of disease tolerance[23]. Collectively, our results indicate that while the toxin is dispensable for the initiation of mucormycosis, it plays a central role in the lethality of this disease.

IgG anti-toxin protected mice from mucormycosis

To further verify the role of the toxin in the pathogenesis of mucormycosis, we infected DKA mice intratracheally with wild-type *R. delemar* and then 24 h later, treated them with a single 30 µg dose of either the IgG anti-toxin or normal rabbit IgG. While mice treated with normal IgG had a mortality rate of 95%, treatment with the IgG anti-toxin resulted in ~70% long-term survival (**Fig. 2d**). Surviving mice appeared healthy and had no detectable fungal colonies in their lungs when the experiment was terminated on day 21. In accord with data from

the fungal burden in tissues of mice infected with the toxin-attenuated strain, antibody treatment had no effect on the fungal burden of lungs or brains when tissues were harvested four days post infection (**Extended Data Fig. 7b**). These data further confirm the role of the toxin in the pathogenesis of mucormycosis and point to the potential of using anti-toxin antibodies to treat the disease.

We also performed histopathological examination of the tissues from all groups of mice sampled at the same time of tissue fungal burden studies (day 4) to gain insight into the mechanism of action of the toxin. While, uninfected mice had normal lung architecture with no signs of inflammation or infection (**Fig. 2e**), lungs from mice infected with *R. delemar* transformed with the RNAi empty plasmid (control) showed fungal and granulocyte infiltration (**Fig. 2f left panel**) and angioinvasion with thrombosis (**Fig. 2f right panel**). In contrast, lungs from mice infected with the toxin-attenuated mutant showed only mild signs of inflammation with no angioinvasion (**Fig. 2g**). Importantly, lungs of mice infected with wild-type *R. delemar* and treated with the IgG anti-toxin showed architecture that was similar to the lungs of the uninfected control mice; there were no signs of inflammation or infiltration with *R. delemar* (**Fig. 2h**).

Down regulation of the toxin gene or treatment with IgG anti-toxin attenuated *R. delemar*-mediated host cell damage *in vivo*

To determine whether the toxin contributed to host cell damage *in vivo*, we used the ApopTag *in situ* apoptosis kit to stain the lung tissues of the infected mice. While extensive lung damage was observed in mice infected with wild-type *R. delemar*, the lungs harvested from mice infected with the toxin-attenuated mutant (**Extended Data Fig. 8a**) or those infected with wild-

type *R. delemar* and treated with the IgG anti-toxin (**Extended Data Fig. 8b**) had almost no detectable damage.

Finally, we have previously reported on a mucormycosis case in a human with disseminated mucormycosis[9]. Haemotoxylin and Eosin (H&E) staining of lung tissues of this patient showed broad aseptate hyphae that caused necrosis and massive infiltration of tissues compared to thinner septated hyphae present in a patient suffering from invasive pulmonary aspergillosis (**Extended Data Fig. 9a,b**). Subsequent immunohistochemistry of the patient's lungs using the IgG anti-toxin (*vs.* control IgG) showed association of the toxin with fungal hyphae and the surrounding tissues in a mucormycosis patient and lack of staining in tissues of an aspergillosis patient (**Extended Data Fig. 9c,d**). These results show that the toxin is also involved in human mucormycosis, is cell-associated as well as secreted/shed into the surrounding tissues, and confirm the specificity of the antibody used in these studies since the putative toxin does not have an orthologue in *Aspergillus* (**Supplementary Table 1)**.

To confirm the secretion/shedding of the toxin, we grew *R. delemar* spores in 96-well plate with or without amphotericin B (AmB) and assayed cell-free supernatants for the presence of the toxin using a sandwich ELISA with an IgG_1 anti-toxin monoclonal antibody that we raised in mice as a capture antibody and the rabbit IgG anti-toxin as the detecting antibody. The toxin was detected in cell-free supernatants of *R. delemar* wild-type (26.7 ± 0.87 nM) or *R. delemar* transformed with the empty plasmid (23.0 ± 2.04 nM), but not in *R. delemar* transformed with RNAi targeting the toxin. In accord with secretion/shedding of the toxin by live hyphae, supernatants collected from wild-type *R. delemar* hyphae in which further growth has been hampered by AmB concentrations ≥ 2 μg/ml showed little to no secretion/shedding of the toxin

(**Extended Data Fig. 10**). These results confirm that the toxin is secreted/shed into the growth medium.

The hyphae-associated toxin has structural features of ricin

Given the critical role of the toxin in the pathogenesis of mucormycosis, we did structural and bioinformatics studies to understand its mechanism of action. As reported in **Supplementary Table 1**, many of the toxin orthologues found in other organisms are annotated as ricin domain-containing proteins or ricin B chain-like lectins. Further detailed bioinformatic analysis of the *R. delemar* toxin sequence showed a two domain structure similar to that of ricin (Sequence ID: NP_001310630.1)[24] (**Fig. 3a**). Specifically, the *R. delemar* toxin harbored a small region (amino acids 198-289) that resembled a sequence in ricin chain A, known to be involved in inactivating ribosomes (*i.e.* ribosome inactivating protein [RIP]), and two domains (amino acids 304-437 and 438-565) of the lectin-binding ricin chain B. Moreover, the *R. delemar* toxin contained an LDV-motif (**Fig. 3a**) that is present in ricin (**Fig 3a**, red colored amino acids) and that has been reported to cause damage to HUVECs *in vitro*[25,26], and *in vivo* in models of vascular leak[27] as well as postulated to cause ricin A chain-mediated vascular leak syndrome in humans[25]. Furthermore, gene ontology studies predicted that *R. delemar* toxin would have functions similar to ricin including sugar binding (GO:0005529, score of 0.64), as well as rRNA glycosylase activity (GO:0030598, score of 0.49) and hydrolase activity (GO:0004553, score of 0.35) (**Fig. 3a**, table).

We produced a 3-D structural model of the *R. delemar* toxin by searching templates within the SWISS-Model template library (SMTL). The greatest resemblance was with sugar-binding proteins, especially galactose, the known lectin for ricin[28]. Other proteins with predicted

resemblance to mucoricin included those with cell adhesion, toxin and hydrolase (glycosylase) activities (**Supplementary Table 2**). The rRNA glycosylase activity is a feature of ricin and is required for inactivating ribosomes[29]. Finally, the structures of the *R. delemar* toxin and ricin B chain were superimposable with a highly significant Tm-align score of 0.81and a score of 0.78 for ricin B domain I (amino acids 304-437) and domain II (438-565 amino acid), respectively (**Fig. 3b)**. However, the 17 kDa *R. delemar* toxin is much smaller than either the A or B chains of ricin (32 kDa each). Nevertheless, the fungal toxin appears to share structural homology with portions of ricin that are responsible for inactivating ribosomes, inducing vascular leak and binding to galactose.

***R. delemar* toxin is immunologically cross-reactive with ricin**

To further explore the similarities between *R. delemar* toxin and ricin, we used the IgG anti-*R. delemar* toxin in an ELISA to determine whether the toxin and ricin were immunologically cross-reactive. Plates were coated with ricin or *R. delemar* toxin, and then incubated with the IgG anti *R. delemar* -toxin, or normal rabbit IgG. The former but not the latter bound to ricin or *R. delemar* toxin in a dose dependent manner **(Fig. 3c**). The IgG anti-*R. delemar* toxin also recognized ricin, and a murine monoclonal antibody (8A1) against the ricin B chain[30] recognized the *R. delemar* toxin in a dot blot (**Fig. 3d**). Furthermore, the IgG anti-*R. delemar* toxin reacted with both the *R. delemar* toxin and ricin in a Western blot (**Fig. 3e**). Importantly, the IgG anti-*R. delemar* toxin protected A549 alveolar epithelial cells from ricin-induced damage in a manner similar to that of the IgG anti-ricin B chain (8A1 clone) or galactose [the lectin for the ricin chain B (**Fig. 3f**)]. Collectively, these data demonstrate the similarities between the two toxins.

Mucoricin is a RIP that also promotes vascular permeability and induces both necrosis and apoptosis of host cells

After ricin is internalized by cells *via* its lectin-binding B chain, it's A chain exerts its toxic activity by irreversibly inactivating ribosomes *via* its N-glycosylase activity. This result in the inhibition of protein synthesis[31]. The enzyme activity cleaves the N-glycosidic bond between the adenine nucleobase in the α-sarcin-ricin loop and its ribose causing the release of adenine (depurination)[32]. To determine whether the *R. delemar* toxin had similar activity, we compared the ability of the two toxins to inhibit protein synthesis in a cell-free rabbit reticulocyte assay[33]. As reported previously[34], ricin concentration that caused 50% inhibition in protein synthesis (IC_{50}) was ~ at 2.2 x 10^{-11} M (**Fig. 4a**). The recombinant toxin of *R. delemar* also inhibited protein synthesis, albeit with ~ 800-fold weaker activity than ricin (*i.e.* an IC_{50} of 1.7 x 10^{-8} M) (**Fig. 4b**). To determine if the protein inhibition is due to depurination, we used HPLC to measure the amount of adenine released from template RNA extracted from A549 alveolar epithelial cells[32]. In contrast to RNA exposed to the buffer control, RNA incubated with mucoricin released detectable amounts of adenine (**Fig. 4c**). The depurination is due to rRNA N-glycosylase activity since in contrast to the negative control, ovalbumin (OVA) which did not cleave 28S rRNA, the *R. delemar* toxin cleaved the rRNA in rabbit reticulocyte lysates after adding aniline, albeit at a concentration of 10^4 higher than ricin and after incubation with the ribosomes for a longer period of time (**Fig. 4d**). Thus, like ricin, the *R. delemar* toxin is a RIP.

In addition to its N-glycosylase activity, ricin chain A is known to cause vascular leak *in vitro*[25,26] and *in vivo*[27] mediated by its LDV sequence, a motif that is also present in the *R. delemar* toxin (**Fig. 3a**). To examine whether the *R. delemar* toxin compromised vascular integrity, we grew HUVECs on membrane inserts in transwells prior to treating the confluent

monolayers with either *R. delemar* spores or *R. delemar* toxin for 5 h at concentrations that did not kill the HUVECs (**Supplementary Fig. 1).** The permeability of HUVECs was determined by measuring the amount of fluorescent dextran migrating from the upper chamber to the lower chamber of the transwells after adding *R. delemar* spores (**Fig. 4e**) or recombinant *R. delemar* toxin (**Fig. 4f**). Both *R. delemar* and the toxin induced permeability, which was equivalent to that induced by *E. coli* lipopolysaccharide (LPS), a potent inducer of vascular permeability[35]. Furthermore, IgG anti-*R. delemar* toxin blocked this enhanced permeability by 50-60%. Importantly, IgG anti-ricin B chain (8A1 clone) almost completely abrogated the permeability induced by *R. delemar* or its toxin (**Fig. 4e,f**). These results confirm that *R. delemar* induces permeability in HUVECs *via* its toxin and that IgG anti-ricin B chain blocks this *R. delemar*-mediated virulence trait.

Ricin is also known to cause cell damage by inducing both necrosis and apoptosis[36,37]. To determine whether the *R. delemar* toxin did the same, we used an Apoptosis/Necrosis detection kit to compare the abilities of *R. delemar* toxin and ricin to damage alveolar epithelial cells. As compared to the control, after 2 h both toxins caused comparable apoptosis and necrosis (**Fig. 4g,h**). Collectively, these results demonstrate the functional similarities between ricin and *R. delemar* toxin as RIPs that inhibits protein synthesis *via* N-glycosylase activity. Both toxins also cause cell death by apoptosis and necrosis. Based on the structural and functional similarity to ricin, we named the *R. delemar* toxin **mucoricin** and the corresponding gene **Ricin-Like Toxin (*RLT1*)**.

Discussion

Mucormycosis is a lethal fungal infection often associated with extensive tissue damage. We have now identified a cell-associated/secreted/shed toxin that is widely present in pathogenic Mucorales fungi. We used genetic and biochemical techniques to show that the toxin gene, *RLT1* and its encoded protein (mucoricin) are required for the full virulence of *R. delemar.* In addition to being produced by pathogenic Mucorales, this toxin appears to be present in other fungi and bacteria. For example, orthologues in *Rhizophagus* were identified to have 30-40% identity with *RLT1*. *Rhizophagus* lives symbiotically with plants and is recognized as an integral part of the natural ecosystem and was shown to delay plant disease symptoms caused by *Phytophthora infestans*[38]. Similarly, *RLT1* orthologues were identified in the bacterial genera of *Streptomyces* and *Paenibacillus* (~30% identity). Both bacteria are known inhabitants of soil, present in rhizosphere of various plants, and are used as biological control agents for crops because of their ability to secrete secondary metabolites[39].

Mucoricin has structural and functional similarities to ricin, a prototypic Type 2 RIP consisting of two polypeptide chains (A and B) that are linked by a disulfide bond[24]. The A-chain of ricin is an *N*-glycosidase that is responsible for inactivating ribosomes, and the B chain is a galactose-specific lectin[29] that enables the toxin to bind to target cells[28]. In contrast, Type I RIPs are monomeric A-chain-like RIPs[29]. Mucoricin appears to have the activities of both ricin A and B chains (and Type I RIPS) and both activities are present in a single 17 kDa protein (**Fig. 3e**). Several other RIPs isolated from plants consist of low molecular weight single chain proteins including a 26 kDa TRIP isolated from tobacco leaves[40] and a 7.8 kDa protein isolated from sponge gourd seeds (*Luffa cylindrica*)[41].

The strong sequence and structural similarity between mucoricin and ricin lies in the ricin B-chain, although mucoricin inhibits protein synthesis *via* N-glycosylase activity leading to

depurination, albeit with lower activity than ricin. A possible explanation for the ability of mucoricin to inhibit protein synthesis is likely predicted by its conserved rRNA glycosidase activity. Specifically, the EAARF motif in ricin A chain is known to be responsible for the RIP activity of ricin. It is known to depurinate adenosine 4324 in 28S rRNA with the glutamic acid residue (E, shaded) responsible for this activity[42]. Furthermore, the arginine residue (R, shaded) separated by two amino acids from the glutamic acid residue (**Fig. 3a**, green brackets), is also required for the activity of the bacterial Shiga toxin, a potent ricin-like A chain with a fully conserved EAARF domain of ricin[43]. Mucoricin has the EEGRL, in which the glutamic acid and arginine residues are conserved (**Fig. 3a**, green brackets).

Another functional domain in ricin and Shiga toxin reported to be required for RIP activity is the WGRLS[44] (**Fig. 3a**, cyan underline). This sequence also aligns with the EEGRL motif of mucoricin (**Fig. 3a**, green brackets; and **Supplementary Table 3**). Furthermore, mucoricin contains the EAANQ motif (**Fig. 3a**, purple overline) which resembles the ricin sequence of EAARF, with the glutamic acid residue conserved and the arginine residue replaced by asparagine, a conserved amino acid with properties that are weakly similar to arginine. The lack of fully conserved functional residues (*i.e*. arginine) between mucoricin and ricin/Shiga toxins likely explains the 800-fold weaker RIP activity of mucoricin as compared to ricin (**Fig. 4a,b**). Finally, mucoricin also has sequence homology with several other RIPs including saporin of *Saponaria officinalis*, a Type 1 RIP with 19% overall identity and 10 out of the 17 conserved amino acid residues in the functional domain of EAARF (**Supplementary Fig. 2**). Notably, the EEGRL and EAANQ are widely present in Mucorales fungi known to cause human disease (**Supplementary Table 3**). Thus, mucoricin appears to be a RIP that functionally resembles ricin

A chain and Type-1 RIPs such as saporin[45]. The contribution of the EEGRL and EAANQ motifs to the RIP activity is being further investigated.

Our *in vitro* studies suggest that *RLT1* is expressed most strongly when the hyphal matt is aeriated and in response to alveolar epithelial cells (**Extended Data Fig. 4c,d**). These results further suggest that mucoricin may be highly active during pulmonary mucormycosis and potentially in rhinoorbital disease, when hyphae are exposed to epithelial cells in the presence of ambient levels of oxygen. It is of interest that, mitochondria are believed to play a central role in RIPs' (e.g. ricin, Shiga toxin and abrin) ability to induce host cell apoptosis[46]. Although the expression of *RLT1* in *R. delemar* is higher in response to alveolar epithelial cells than to HUVECs (**Extended Data Fig. 4d**), the latter host cells are damaged much more rapidly by *R. delemar* (*i.e.* significant *R. delemar*-induced HUVEC injury occurs at 8 h *vs.* 48 h for *R. delemar*-induced alveolar epithelial cells [**Extended Data Fig. 1**])[13], and by purified mucoricin (**Fig. 1a**). In accord with these results, it has been shown that HUVECs are rapidly damaged and their permeability affected by small peptides containing the LDV-motif but lacking the sequences responsible for N-glycosidase activity[26]. In this study we show that *R. delemar* compromises the permeability of HUVEC monolayers *in vitro* by the direct effect of mucoricin. The LDV and other (x)D(y) motifs (with known vascular leak effector function) are widely present in pathogenic Mucorales **(Supplementary Table 3**)[25]. Thus, it is possible that the LDV-motif is responsible for angioinvasion and rapid hematogenous dissemination in mucormycosis[6] by inducing damage to vascular endothelial cells.

The exact mechanism by which mucoricin enters a target cell to exert its lethal effect is not yet known. However, our data strongly indicate that it is cell-associated as well as secreted/shed by Mucorales. The amount of toxin in the medium (27 nM, **Extended Data Fig.**

412 **10b**) from a small-scale growth in a 96-well plate was sufficient to exceed the IC_{50} in RIP
413 activity of 17 nM (**Fig. 4b**). Thus, secreted/shed toxin likely exerts its toxicity by binding to and
414 then entering the host cells in the absence of invading hyphae. Alternatively, invading *R.*
415 *delemar* hyphae release the toxin once they are phagocytosed by immune[9] cells or barrier
416 cells[13,47,48].

417 Our *in vivo* studies clearly demonstrate the contribution of mucoricin to pathogenesis by
418 enhancing angioinvasion, inflammation and tissue destruction. There is also evidence that the
419 lethality of ricin *in vivo* is related at least in part to its ability to induce a massive inflammatory
420 immune response accompanied by infiltration of PMN[49] in many settings such as acute lung
421 injury[49,50] and gastrointestinal disease[51]. This is likely due to activation of the innate arm of the
422 immune system by the toxin itself or by toxin-damaged cells. Indeed, our histopathological
423 examination of organs harvested from mice injected with purified mucoricin shows inflammation
424 and recruitment of PMNs (**Fig. 1e**). Neutralizing the effect of the toxin either by RNAi or by
425 anti-mucoricin antibodies decreased inflammation and host tissue damage (**Fig. 2e-h** and
426 **Extended Data Fig. 8**). These results confirm the critical role of mucoricin in the pathogenesis
427 of mucormycosis and suggest that it is involved in mediating inflammation and tissue damage,
428 both of which are clinical features of mucormycosis. Of note, treatment of mucormycosis
429 patients with antifungal agents is often hampered by the extensive tissue necrosis that prevents
430 optimal delivery of drugs into the site of infection. Hence, antifungal treatment alone (without
431 surgical intervention) is often non-curative[6]. Thus, antibody-mediated neutralization of
432 mucoricin might reduce tissue necrosis, decrease the need for disfiguring surgery, and maximize
433 the effect of antifungal therapy.

Based on these results, we propose a model of pathogenesis and the role of mucoricin in this process. We suggest the following events.

i. Infection is initiated when fungal spores are inhaled, and in the absence of phagocytes (or presence of dysfunctional phagocytes such as in patients with DKA). Fungal spores express CotH[10-12] and bind to either GRP78 on nasal epithelial cells[48], or to integrin β1[48] which activates epidermal growth factor receptor (EGFR)[47] on alveolar epithelial cells to induce invasion.

ii. Under aerobic conditions, the calcineurin pathway is activated in the inhaled spores, causing them to germinate[52,53], a process that leads to the production of mucoricin.

iii. Mucoricin binds to tissue cells by its lectin receptor, inhibits protein synthesis, and causes apoptosis and necrosis. The toxin can also compromise vascular permeability resulting in rapid hematogenous dissemination and tissue edema often seen in patients with mucormycosis.

iv. While tissue damage is occurring, and because the toxin and debris from necrotic cells are recognized by the immune system, an inflammatory immune response leads to the recruitment of PMNs and other tissue-resident phagocytes.

v. Although the recruited phagocytes damage some of the invading hyphae, both the dead and live hyphae release mucoricin, resulting in more host cell death and more inflammation.

vi. In the necrotic tissue, the fungus can proliferate, protected from both phagocytes and anti-fungal drugs.

Our finding that mucoricin remains active even in dead organisms offers an explanation for why antifungal therapy alone has limited efficacy in patients with mucormycosis, and why

457 the fungal lesions must frequently be surgically excised. Importantly, other toxins/mechanisms
458 of host cell damage likely exist in Mucorales, since antibody blocking studies and
459 downregulation of toxin gene expression do not fully abrogate the ability of *R. delemar* to
460 damage host tissues**.**

461 In summary, we have identified a ricin-like toxin (mucoricin) that is widely present in
462 Mucorales fungi, where it plays a central role in the pathogenesis of mucormycosis. We postulate
463 that strategies to neutralize mucoricin will have significant therapeutic benefits.

Correspondence and requests for materials should be addressed to Ashraf S. Ibrahim: ibrahim@lundquist.org

Acknowledgments

This work was supported by a Public Health Service grant R01AI063503 and R01AI141360 to ASI. MS is supported by R00DE026856, ESV by R01A11752861, VMB by U19AI110820 and R01AI141360, and SGF by R01AI124566 and R01DE022600. ESV is also supported by the Simmons Patigian Distinguished Chair and a Distinguished Teaching Chair. AR is sponsored by the SURF program at UT Southwestern and is currently at Vanderbilt University.

We would like to thank Dr. Samuel French for his assistance in reading the histopathological slides of the purified mucoricin, Ms. Heewon Jeon, Ms. Ayesha Ahmed, and Mr. Stephen Ruback for technical assistance. We thank Dr. David Vance and Ms. Greta Van Slyke for their work on the 8A1 monoclonal antibody and Dr. Robert Munford, NIH for his insightful suggestions concerning the nature of the toxin.

Author contributions

S.S.M.S. conceived, designed and performed studies to purify and identify the toxin, and screen its activity *in vitro* and *in vivo* and wrote the manuscript. C.B. generated mucoricin mutants and characterized their virulence *in vitro* and *in vivo* and conducted the antibody efficacy studies. Y.G. helped in animal studies, conducted confocal microscopy, cross reactivity studies, and RIP activity studies. S.S. designed and performed homology modeling, cross reactivity studies, and toxin secretion studies. T.G. helped in the animal studies. M.S. performed the necrosis/apoptosis assay and the mouse immunohistochemistry studies. A.A. performed permeability studies,

E.G.Y. performed sequence alignment and gene ontology studies. S.A. purified recombinant toxin and polyclonal antibodies. A.P. and G.C. provided and performed the human immunohistochemistry studies. C.P. and V.V. performed and interpreted the mouse histology studies. AR carried out studies on cross-reactivity of mucoricin and ricin. V.M.B. and J.D.H. performed phylogenetic studies and blast search of mucoricin in Mucorales. N.J.M. generated and characterized the 8A1 monoclonal antibody. J.E.E. and S.G.F. provided intellectual advice, designed studies, and edited the manuscript. E.S.V. conceived, designed and carried out studies of cross reactivity, provided reagents and expertise on ricin and helped write the manuscript. A.S.I. conceived, designed, coordinated and supervised the studies, performed experiments, analyzed data, and wrote the manuscript along with comments from co-authors.

Materials and Correspondence:

Reprints and permissions information is available at www.nature.com/reprints

Competing interests

A.S.I. owns shares in Vitalex Biosciences, a start-up company that is developing immunotherapies and diagnostics for mucormycosis. The remaining authors declare no competing interests.

The Lundquist Institute has filed intellectual property rights concerning mucoricin. Vitalex Biosciences has an option to license the technology from The Lundquist Institute for Biomedical Innovation.

Other authors declare no conflict of interest.

Correspondence and requests for materials should be addressed to ibrahim@lundquist.org.

Methods

Organisms, culture conditions and reagents. *R. delemar* 99-880 and *R. oryzae* 99-892 were isolated from the brain and lungs of patients with mucomycosis and obtained from the Fungus Testing Laboratory, University of Texas Health Science Center at San Antonio which had its genome sequenced[19]. *Cunninghamella bertholletiae* 182 is a clinical isolate and is a kind gift from Thomas Walsh (Cornell University). *Lichtheimia corymbifera* is also a clinical isolate obtained from the DEFEAT Mucor clinical study[54]. *R. delemar* M16 is a *pyrf* null mutant derived from *R. delemar* 99-880 and was used for transformation to attenuate mucoricin expression[55]. The organisms were grown on potato dextrose agar (PDA, Becton Dickinson) plates for 5-7 days at 37ºC. For *R. delemar* M16, PDA was supplemented with 100 mg/ml uracil. The sporangiospores were collected in endotoxin free Dulbecco's phosphate buffered saline (PBS) containing 0.01% Tween 80, washed with PBS, and counted with a hemocytometer to prepare the final inoculum. To form germlings, spores were incubated in YPD (Becton Dickinson) medium at 37ºC with shaking for different time periods. Finally, for growth studies 10^5 spores of *R. delemar* wild-type, or mutant strains were plated in the middle of PDA agar plates. The plates were incubated at 37ºC and the diameter of the colony was calculated every day for 6 days. The monoclonal anti-ricin B chain antibody (clone 8A1)[30] and affinity purified rabbit anti-ricin antibodies were prepared and characterized in the Vitetta and Mantis laboratories. Galactose was obtained from Fisher Scientific (Cat # BP656500) and used for blocking the damaging effect of ricin holotoxin.

Host cells. Human alveolar epithelial cells (A549 cells) were obtained from a 58-year-old male Caucasian patient with carcinoma and procured from American Type Culture Collection

(ATCC). The cells were propagated in F-12K Medium developed for lung A549 epithelial cells. Primary alveolar epithelial cells were obtained from ScienCell (Cat # 3200) and propagated in Alveolar Epithelial Cell Medium (Cat#3201) and passaged once.

HUVECs were collected by the method of Jaffe *et al.*[56]. The cells were harvested by using collagenase and were grown in M-199 (Gibco BRL) enriched with 10% fetal bovine serum, 10% defined bovine calf serum, L-glutamine, penicillin, and streptomycin (all from Gemini Bio-Products, CA). Second-passage cells were grown to confluency in 24- or 96-well tissue culture plates (Costar, Van Nuys, CA) on fibronectin (BD Biosciences). All incubations were in 5% CO_2 at 37ºC. The reagents were tested for endotoxin using a chromogenic limulus amebocyte lysate assay (BioWhittaker, Inc.), and the endotoxin concentrations were less than 0.01 IU/ml.

Fresh red blood cells were isolated from blood samples collected from healthy volunteers after obtaining a signed informed consent form and processed as previously described[57]. Endothelial cell and red blood cell collection was approved by Institutional Review Board at The Lundquist Institute at Harbor-UCLA Medical Center.

Purification and characterization of ricin. Two sources of ricin were used. One was purified from a large stock of pulverized castor beans in the Vitetta laboratory[58]. Its IC_{50} and toxicity were tested on Daudi lymphoma cells (ATCC® CCL-213™), HUVECs, and in cell free reticulocyte assays[25,34,59]. The other source was purchased from Vector Laboratories (Burlingame, CA; Cat No. L-1090). Both sources were similar in purity and activity.

555 **Purification and identification of mucoricin.** To purify mucoricin, *Rhizopus* fungal spores
556 (10^3/ml) were grown for 5 days at 37^{o}C in YPD culture medium. The supernatant was separated
557 from the fungal mat by filtration and the fungal mycelia was ground in liquid nitrogen and
558 extracted with sterile water, concentrated and analyzed through size exclusion columns[15]. Host
559 cell damage assay showed that substances >10 kDa and < 30kDa is responsible for injuring the
560 host cells (**Extended Data Fig. 1a**). The concentrated water extract was then subjected to 3D
561 chromatographic separations (**Extended Data Fig. 1**). For the first dimension, the concentrated
562 extract run on native polyacrylamide gel under electrophoretic force (**Extended Data Fig. 1b**).
563 The gel was cut into 6 pieces and then eluted separately in PBS buffer prior to testing for their
564 damaging activity. Only fraction #6 corresponding to 15-20 kDa showed damaging effect to host
565 cells (**Extended Data Fig. 1c**). Next, this fraction was concentrated and subjected to separation
566 using methanol:water (4:1) as a solvent on cellulose plates. Fractions were scraped from the
567 cellulose plate and dissolved in irrigation water, followed by incubation with host cell after filter
568 sterilization. A third dimensional fractionation was applied to the fraction that caused damage
569 using cellulose plates and with the solvent system as above. This round of fractionation resulted
570 in one fraction causing damage to host cells.
571
572 **Structural modeling of mucoricin.** For amino acid sequence comparisons, mucoricin and ricin
573 (Sequence ID: NP_001310630.1) protein sequences were aligned using MUSCLE/CLUSTAL-
574 W. We searched the SWISS-MODEL template library (SMTL) (https://swissmodel.expasy.org/)
575 to find templates for building 3-D structural model of mucoricin. Briefly, a BLAST search of the
576 SMTL against the primary amino acid sequence identified the target sequence. To build the
577 model, we performed target-template alignment using ProMod3, and templates with the highest

quality were selected for model building. Insertions and deletions were re-modeled using a fragment library, and the side chains were rebuilt. Finally, the geometry of the resulting model is regularized by using a force field. In case loop modeling with ProMod3 fails, an alternative model is built with PROMOD-II. The models showing high accuracy values were finalized for similarity comparisons. Ricin 3-D structure models were also built using ricin chain B amino acids 313-435 and 440-565[60-62]. Ricin and mucoricin 3-D protein models were aligned using MacPyMOL software and Tm align score was calculated by webtool Tm Align (https://zhanglab.ccmb.med.umich.edu/TM-align)[63]. Using gene ontology term prediction, mucoricin was predicted to have carbohydrate-binding, hydrolase activity and negative regulation of translation functions.

Expression and purification of mucoricin. Heterologous expression of mucoricin gene in *S. cerevisiae* was performed to ensure the production of a functional toxin since we used this yeast to generate functional *R. delemar* proteins before[11,64]. The heterologous expression was conducted as follows; total RNA was isolated from *R. delemar* hyphae grown on YPD broth and reverse transcribed into cDNA. The entire ORF of mucoricin was PCR amplified from cDNA using Phusion High-Fidelity PCR Kit (New England Biolabs) using the primers 5'-GATAAG**ACTAGT**ATGTATTTCGAAGAAGGC-3' and 5'-GGTGATG**CACGTG**TCCTTCAAATGGCACTA-3'. The amplified PCR product was verified by sequencing and then cloned into modified XW55 yeast dual expression vector[65] in the highlighted *Spe*I and *Pml*I sites downstream of the ADH2 promoter by yeast recombinase technology [protocolYeastmaker™ YeastTransformation System 2 (Clontech)] and according to the manufacturer's instructions. The generated yeast expression vector was transformed into *S.*

601 *cerevisiae* strain BJ5464 using protocol Yeastmaker™ Yeast Transformation System 2
602 (Clontech). The transformants were screened on yeast nitrogen base (YNB) medium lacking
603 uracil. *S. cerevisiae* transformed with empty plasmid was served as negative control.
604 Transformants were grown on YNB without uracil for 1-3 days then transformed into YPD
605 medium for 3 days at 30^{o}C with shaking. The expression of mucoricin was induced once the
606 glucose was exhausted from the medium and yielded a recombinant mucoricin that was both 6x
607 His- and Flag-tagged. Purification of the recombinant mucoricin was performed by Ni-NTA
608 matrix affinity purification according to the manufacturers' instructions (Sigma-Aldrich). The
609 purity of the protein was confirmed by SDS-PAGE and quantified by a modified Lowry protein
610 assay (Pierce).
611
612 **Anti-mucoricin and anti-ricin antibodies.** Rabbit and mouse monoclonal antibodies against
613 recombinant mucoricin coupled to KLH were raised by ProMab Biotechnologies Inc.[11]. The IgG
614 fraction was purified from the antisera using protein A/G spin column (Thermo Fisher Scientific)
615 according to the manufacturer's instructions. Normal IgG was purified from the sera of non-
616 immunized rabbits and used as a control. Rabbit and monoclonal antibodies against ricin and
617 ricin B chain were prepared as described previously[27,30]. Hybridoma cells producing anti-
618 muroricin antibodies were propagated in WHEATON CELLine bioreactor 350 using protein-free
619 hybridoma medium 1× (Gibco) for 5 to 7 days at 37°C in 5% CO_2. The antibody-containing
620 supernatant was collected and purified using protein G spin columns (Thermo Fisher Scientific).
621 Eluted purified IgG were dialyzed in PBS using a dialysis cassette (Thermo Fisher Scientific),
622 and the purity of the antibodies was confirmed by SDS-PAGE prior to determining the
623 concentration using the Bradford protein assay (Bio rad, Hercules, CA). Endotoxin levels were

624 measured by the Limulus Amebocyte Lysate (LAL) kit (Charles River) and determined to be
625 <0.8 EU/ml which is below the 5 EU/kg body weight set for intraperitoneal injection[66].
626 Mouse monoclonal antibody clone 8A1 was raised against the ricin B chain[30], which has 33%
627 sequence identify with mucoricin. Clone 8A1 recognizes an epitope mapped to ricin B chain (2γ,
628 amino acids 221-262).
629
630 **Cell damage assay**. The damage of epithelial cell [A549 and Primary (ScienCell, Cat # 3200)]
631 and HUVECs was quantified using a ^{51}Cr-release assay[67]. Briefly, confluent cells grown in 24-
632 well tissue culture plates were incubated with 1 μCi/well $Na_2{}^{51}CrO_4$ (ICN) in F12K-medium (for
633 epithelial cells) or M-199 medium (HUVECs) for 16 h. On the day of the experiment, the media
634 was aspirated, and cells were washed twice with pre-warmed Hanks' balanced salt solution
635 (HBSS, ScienCell). Cells were treated with toxin suspended in either 1 ml of F12K-medium (for
636 epithelial cells) or RPMI 1640 medium (for endothelial cells) supplemented with glutamine and
637 incubated at 37°C in a 5% CO_2 incubator. Spontaneous ^{51}Cr release was determined by
638 incubating the untreated cells in the same volume of the culture medium supplemented with
639 glutamine. At different time points, and after data were corrected for variations in the amount of
640 tracer incorporated in each well, the percentage of specific cell release of ^{51}Cr was calculated as
641 follows: [(experimental release) – (spontaneous release)]/[1 – (spontaneous release)][68]. Each
642 experimental condition was tested at least in triplicate, and the experiment was repeated at least
643 once.
644 In some experiments, the effect of mucoricin gene silencing on damage to HUVECs or
645 A549 cells was measured by incubating 1.0 x 10^6/ml or 2.5 x 10^5/ml spores of *R. delemar* and
646 incubated for 6 or 48 h, respectively. In other experiments the protective effect of IgG anti-

mucoricin was measured by incubating the fungal cells with either 50 μg/ml of IgG anti-mucoricin or normal rabbit IgG (R & D Systems, Cat # AB-105-C) for 1 h on ice prior to adding the mixture to A549 cells radiolabeled with ^{51}Cr. The assay was carried out for 48 h. The amount of damage was quantified as above.

To study the effect of fungal cell viability on host cell damage, fungal spores (10^6/ml) were cultured in F12K media and left to grow overnight at 37^{o}C. The fungal hyphae were collected by filtration, dried by padding with a sterile filter paper, weighed and then aseptically cut into four equal small pieces of 0.1 mg wet weight. The fungal hyphal matt was suspended in 1 ml F12K and heated at 60^{o}C in a water bath for 4 h and then cooled down. To check the viability of the hyphal matt, a loop full of the hyphae was plated on PDA plates. The other two groups of fungal hyphae were suspended in preheated and cooled in F12K culture media. Another group of F12K culture media was prepared by heating at 60^{o}C and then cooled to represent spontaneous control. The fungal samples were incubated with ^{51}Cr-labelled A549 alveolar epithelial cells previously seeded into 24-well plates as above and the damage assay was carried out for 24 h at 37^{o}C and the amount of ^{51}Cr released in the supernatant was measured as above.

To determine whether IgG anti-mucoricin protected cells against ricin-induced damage, 5 μg/ml (~77 nM) of ricin was incubated with either 10 μg/ml of the monoclonal IgG anti-ricin B chain (clone 8A1)[69], 10 μg/ml of IgG anti-mucoricin, or normal rabbit IgG (R & D Systems, Cat # AB-105-C) or 10 mM of galactose on ice for 1 h prior to adding to ^{51}Cr-labelled confluent A549 alveolar epithelial cells in 24-well plate. The damage assay was conducted as above for 24 h.

Western blotting. Hyphal expression of mucoricin was determined in *R. delemar* wild-type, or RNAi mutants from hyphal matt grown for overnight at 37^{o}C in YNB without uracil medium[70]. Briefly, mycelia were collected by filtration, washed briefly with PBS, and then ground thoroughly in liquid nitrogen using mortar and pestle for 3 min. The ground powder was immediately transferred to microfuge tube containing 500 µl extraction buffer which consisted of 50 mM Tris-HCl, pH 7.5, 150 mM NaCl, 10 mM $MgCl_2$. The extraction buffer was supplemented with 1X Halt Protease Inhibitor Cocktails (Thermo Scientific) and 1 mM phenylmethylsulfonyl fluoride (PMSF). The sample was vortexed vigorously for 1 min, then centrifuged for 5 min at 21000 g at 4^{o}C. The supernatant was filtered with PES syringe filters (Bioland Scientific, Cat# SF01-02) and transferred to a new tube and the protein concentration determined using Bradford method.

For Western blotting, 10 µg of each sample was used to separate proteins on an SDS-PAGE. Separated proteins were transferred to PVDF membranes (GE Water & Process Technologies) and treated with Western blocking reagent (Roche) for overnight at 4^{o}C. The IgG anti-mucoricin (2 µg/ml) and the murine 8A1 monoclonal anti-ricin B chain were used as primary antibodies. After 1 h, 0.5 µg/ml of HRP- IgG anti-rabbit IgG (Jackson ImmunoResearch, Product number 111-035-144) (when rabbit IgG anti-mucoricin was used as a primary) or HRP-IgG anti-mouse (Invitrogen, Cat #31450) (when murine 8A1 antibody anti-ricin B chain used as a primary) secondary antibodies (Jackson Immuno Research) were added for another 1 h at room temperature. Mucoricin bands were visualized by adding the HRP substrate (SuperSignal West Dura Extended Duration Substrate, Thermo Scientific), and the chemiluminescent signal was detected using an In-gel Azure Imager c400 fluorescence system (Azure Biosystems). The intensity of the bands was quantified by ImageJ software.

693 To examine the cross reactivity of ricin with IgG anti-mucoricin, 5 µg of ricin (77 pmol) or
694 recombinant mucoricin (294 pmol) were submitted to SDS-PAGE under reducing and denaturing
695 conditions. Western blotting was conducted as above using IgG anti-mucoricin as a primary
696 followed by HRP- IgG anti-rabbit IgG as secondary (Jackson ImmunoResearch, Product number
697 111-035-144).
698
699 **Gene expression analysis**. Expression of the mucoricin gene was studied in *R. delemar* as
700 spores (10^3/ml) germinated into hyphae in YPD medium for 16 h at 37ºC. At selected times, cells
701 or mycelia were collected by centrifugation, followed by filtration using 0.22 µm membrane
702 units. The cells were washed once with PBS, and ground in liquid nitrogen using mortar and
703 pestle. RNA was extracted using RNeasy Plant Mini kit (Qiagen). To quantify the expression
704 of the mucoricin gene in response to host cells, fungal spores (10^6/ml) were incubated with either
705 epithelial, HUVECs or human erythrocytes in 24-well plate using F12K, RPMI, or PBS,
706 respectively. The fungal cells were collected at different time intervals including zero, 2 and 5 h
707 and directly ground with liquid nitrogen followed by RNA extraction using RNeasy Plant Mini
708 Kit. Contaminating genomic DNA was removed from RNA samples by treatment with 1 µl of
709 Turbo-DNase (Ambion) for 30 min at room temperature. DNase was then removed using an
710 RNA Clean-Up kit (Zymo Research). First-strand cDNA synthesis was performed using the
711 Retroscript first-strand synthesis kit (Ambion). Toxin specific primers were designed with the
712 assistance of online primer design software (Genscript). Mucoricin gene primers include G7F1;
713 5'-CTGGCGTTACGAAAATGGTT-3' and G7R1; 5'-TAAATCAGGACGGGCTTCAC-3'. The
714 amplification efficiency was determined by serial dilution experiments, and the resulting
715 efficiency coefficient was used for the quantification of the products [71]. Gene expression was

716 analyzed by an ABI Prism 7000 Sequence Detection System (Applied Biosystems) using the
717 QuantiTect Sybr Green PCR kit (Qiagen). PCR conditions were 10 min at 90°C and 40 cycles of
718 15 s at 95°C and 1 min at 60°C. Single PCR products were confirmed with the heat dissociation
719 protocol at the end of the PCR cycles. The amount of gene expression was normalized to
720 actin [ACT1-RT5′; 5'-TGAACAAGAAATGCAAACTGC-3' and ACT1-RT3′; 5'-
721 CAGTAATGACTTGACCATCAGGA-3'] and then quantified using the $2(-\Delta\Delta C(T))$ method [72].
722 All reactions were performed in triplicate, and the mixture included a negative no-reverse
723 transcription (RT) control in which reverse transcriptase was omitted.
724
725 ***In vitro* apoptosis/necrosis assay.** A549 lung epithelial cells were grown to confluency on
726 fibronectin-coated circular glass coverslips in 24-well tissue culture plates and then incubated
727 with 50 μg/ml (2.9 μM) mucoricin or 5 μg/ml (77 nM) ricin (concentrations shown to cause *in*
728 *vitro* damage to alveolar epithelial cells [**Fig. 3f**]) for 2 hours after which the cells were washed
729 and stained with 1x Apoxin Green Indicator and 1x 7-AAD (Apoptosis/Necrosis detection kit,
730 Abcam) for 45 min. The cells were fixed and mounted in ProLong Gold antifade containing
731 DAPI (Life Technologies) to visualize cells. Microscopic z-stack pictures were taken using a
732 Leica SP8confocal laser scanning platform. Apoptotic cells *vs.* necrotic cells were identified by
733 their green and red fluorescence, respectively. The number of apoptotic and necrotic events per
734 high-power field (HPF) was determined, counting 10 HPF per coverslip. The experiment was
735 performed three times in triplicate.
736
737 ***In vitro* protein translation assay.** The ability of the two toxins to inhibit protein synthesis was
738 measured by using a modification of a previously described method[33]. Briefly, a rabbit

reticulocyte lysate (Promega, Cat: L4151) was thawed at 37°C immediately before use and supplemented with 40 µl of 1 mM hemin stock solution and 10 µl of 1 M creatine phosphate (Sigma-Aldrich, Cat: 27920) and 10 µl of 5 mg/ml creatine phosphokinase (Sigma-Aldrich, Cat:C7886) before the lysate had fully thawed. The reaction mixture was prepared into 96-well plates as follows: 1 µl of 1 mM amino acid mixture minus methionine (Promega, Cat: L9961), 35 µl of rabbit reticulocyte lysate, 1 µl of 7-fold dilutions of ricin, mucoricin, control OVA, or cycloheximide (Fisher Scientific, Cat: AC357420010). Diluted distilled water was added to a final volume of 48 µl. Two replicates were employed in all experiments and the experiments were repeated at least three times. After a pre-incubation period of 30 min at 37°C, 2 µl ^{35}S Methionine (1,200 Ci/mmol) (PerkinElmer) was added to a final volume of 50 µl. The 96-well plate was incubated at 30°C for 60 min. Two µl from each well was added per well of a 24-well plate containing 98 µl of 0.5 M H_2O_2. Proteins were precipitated with 900 µl of 25% trichloroacetic acid (TCA) before harvesting precipitates on Whatman filter strips (Sigma-Aldrich, Cat: WHA1823035). Filter paper disks were placed in Biofluor scintillation fluid (Perkin Elmer, Cat: 6013329), and [^{35}S] Methionine incorporation was quantitated by scintillation counting. Background counts determined from well containing all reagents without rabbit reticulocyte lysate were subtracted from all CPMs.

The depurination activity assay of mucoricin. The depurination activity of mucoricin was measured by the release of adenine when mammalian RNA was treated with mucoricin for 24 h at 37^{o}C[32]. Mammalian RNA extracted from A549 alveolar epithelial cells by Qiagen RNasy mini kits according to manufacturer's instruction were treated with 20 µg/ml of mucoricin in 0.01M HEPES/10 mM ammonium acetate buffer containing 1 mg/ml BSA for 24 h at 37^{o}C. The solution

was then filtered through a 10 kDa size exclusion column and 40 µl was injected into HPLC using Phenomenex Luna C18 reverse phase column (10 x 250 mm) attached to a Varian ProStar HPLC 218 system (Varian, Walnut Creek, CA). Solvent A was 20 mM ammonium acetate, and solvent B was 100% acetonitrile. The column gradient was as follows: 97% to 60% solvent A in 10 min at flow rate of 1 ml/min. The column effluent was monitored at 260 nm.

Glycosylase activity assay. The N-glycosylase activity of toxins were determined by using rabbit reticulocyte lysate[73,74]. Briefly, 40 µl of lysate was incubated with ricin (1 nM), mucoricin (10 µM) or control OVA (1 nM or 10 µM) in the presence of 10 mM $MgCl_2$ at 30ºC for 1 or 4 hours. After the treatment, ribosomal protein was denatured by 50 mM Tris/0.5% SDS to release RNA. The RNA was purified by phenol-Tris extraction followed by ethanol precipitation. Half of each purified RNA sample was subjected to 2 M aniline acetate (pH 4.5) treatment for 10 minutes on ice, while the other half of RNA was incubated without aniline treatment. rRNA were further extracted using water saturated ether followed by ethanol precipitation. Three micrograms of each rRNA sample were resolved on 7 M Urea Polyacrylamide gel electrophoresis and RNA fragment bands were visualized by staining with ethidium bromide.

Transwell permeability assay[75]. HUVECs were seeded on 24-Corning transwell plate with permeable polyester inserts (0.4 µm, Fisher) coated with fibronectin (15 µg/ml in PBS, Fisher). HUVECs were grown to confluency in M-199 medium with phenol red. *R. delemar* spores (10^5) in M-199 (without phenol red) were added to the upper chamber, and the plate was incubated for 5 h at 37ºC. As a positive control for the permeability of HUVECs, *E. coli* LPS (Sigma-Aldrich) was added at 2 µg/ml to uninfected HUVECs. Following incubation, 3 µl of 50 mg/ml FITC-

785 dextran-10K (Sigma) was added to the upper chamber of the trans-well and the migration of the
786 dextran through the HUVEC monolayer to the lower trans-well was determined 1 h later by
787 quantifying the concentration of the dye in the bottom chamber using florescence microplate
788 reader at 490 nm[75]. To determine the direct effect of mucoricin on the permeability of the
789 HUVEC monolayer, 50 μg/ml (2.9 μM) mucoricin or control OVA were added to the HUVEC-
790 seeded wells instead of *R. delemar*. To determine the effect of antibodies on permeability
791 induced by *R. delemar* or mucoricin, 50 μg/ml of normal rabbit IgG (R & D Systems, Cat # AB-
792 105-C), IgG anti-mucoricin, or 10 μg/ml of IgG anti-ricin toxin chain B (clone 8A1) were
793 incubated for 30 min on ice with *R. delemar* spores or mucoricin prior to their addition to the
794 upper chamber of the trans-well.
795
796 ***In vivo* effects induced by mucoricin.** To test the effect of the purified toxin *in vivo*, male (ICR
797 mice, ~27-32g) were immunosuppressed by intraperitoneal injection of 200 mg/kg of
798 cyclophosphamide and subcutaneous injection of 250 mg/kg cortisone acetate on day −2 and +3,
799 relative to toxin injection. This regimen results in approximately 10 days of leucopenia with
800 reduction in neutrophils, lymphocytes and monocytes as described previously[76]. Mouse gender
801 has no effect on the pathogenesis of mucormycosis, or antifungal treatment as determined by an
802 NIH Contract No. HHSN272201000038I/Task Order HHSN27200008, unpublished data. Mice
803 were given irradiated food and sterile water containing 50 μg/ml baytril (Bayer) ad libitum. 100
804 μl of purified mucoricin (0.1 mg/ml) was then injected into the tail vein on days 0, +2, and +4.
805 The differences in survival between normal mice receiving vehicle (*i.e.* PBS) and those received
806 toxin were compared by the Log Rank test. The primary efficacy endpoint was time to
807 morbidity.

Mouse tissues were fixed in 10% $ZnCl_2$ formalin solution prior to histopathological examination. The fixed organs were dehydrated in graded alcohol solutions, embedded in paraffin, and 5-µm sections were cut and stained with H&E[77]. Cumulative histopathological scores of hemorrhages, neutrophil infiltration (inflammation), and edema were used to determine the effects of toxin by observing 5 fields per slide. The observer was not told the origin of the samples.

Mucoricin RNAi knockdown. RNAi knockdown of mucoricin was employed using our previously described RNAi method[20]. Briefly, a 330-bp mucoricin transcript was PCR amplified using 5'-AAATTTAAAAGCATGCACACACAAAAGTATGAAGATTGCT-3' and 5'-CTGCTTACCATGGCGCGCCCAAATGGCACTAATTCCCAGC-3' primers and cloned into the *Sph*I and *Asc*I sites of pRNAi-pdc[78]. The inverted repeat fragment was PCR amplified by 5'-TTAAGCGATCGCTAGCACACACAAAAGTATGAAGATTGCT-3' and 5'-TTATTCTTATAGCCCGCGGCAAATGGCACTAATTCCCAGC-3' at cloned downstream the intro fragment at the *Nhe*I and *Sac*II sites. The developed construct was transformed into *R. delemar* pyrF mutant (strain M16)[55] using the biolistic delivery system (BioRad), and the homogenous transformants were selected on minimal medium lacking uracil[11]. The down regulation of mucoricin expression was confirmed by qRT-PCR using primers 5'-CTTGGATATCCGTGGAGGTGA-3' and 5'-GGCAGCTTCTTCGACCATCT-3' as described before[12] and by confocal microscopy using immunostaining (see below)[11].

Secretion/shedding of mucoricin into the culture supernatant. Wild-type *R. delemar* spores (2×10^4/100 µl/well), *R. delemar* transformed with the empty plasmid or those transformed with mucoricin RNAi were grown in 96-well plates for 24 h at 37°C followed by additional 24 h of

incubation in the presence or absence of 2-fold serially diluted amphotericin B (0.06-32 μg/ml). 100 μl of culture supernatant samples from each well were collected and stored at -20℃ until used for toxin detection by ELISA. To determine corresponding fungal growth, 100 μl/well XTT substrate (0.20 mg/ml activated with 6.25 μM menadione) was added to the remaining *R. delemar* culture plate.[79] After a 2 h incubation at 37℃, absorbance at 450 nm was measured for metabolized XTT. Sandwich ELISAs were used to detect and quantify mucoricin in the cell-free supernatants. Briefly, 96-well plates were coated with 2 μg/ml mouse anti-*R. delemar* toxin monoclonal antibodies at 4℃ overnight. After washing the plate with 1X PBST (PBS+ 0.05% Tween-20) 5 times, diluted recombinant mucoricin or undiluted culture supernatant samples were added to the ELISA plate. Bound mucoricin was detected by the IgG anti-toxin antibodies (2 μg/ml), and subsequently by HRP- IgG anti-rabbit IgG (Jackson ImmunoResearch, product number 111-035-144) and a TMB substrate detection system (Invitrogen). A standard curve was generated using linear regression of OD_{450} of known recombinant mucoricin concentrations and the concentrations of toxin in the medium were extrapolated from the standard curve.

Confocal microscopy. IgG anti-toxin was used to localize the toxin in the *Rhizopus* fungus[10]. Fungal spores (10^5/ml) were pre-germinated in YPD media at 1, 4, or 12 h. Each fungal stage was fixed in 4% paraformaldehyde followed by permeabilization for 10 min in 0.1% Triton X-100. The permeabilized fungal growth stages were incubated with the IgG anti-toxin for 2 h at room temperature. The fungal stages were then washed 3 times with Tris-buffered saline (TBS, 0.01 M Tris HCl [pH 7.4], 0.15 M NaCl) containing 0.05% Tween 20 and counterstained with anti-rabbit IgG Alexa Fluor 488 (Life Technologies, Cat # A-11034). The stained fungi were imaged with Leica confocal microscope at excitation wavelength of 488 nm. The final confocal

855 images were produced by combining optical sections taken through the z axis.

856

857 ***In vivo* virulence studies and immunohistochemistry.** Male ICR mice (≥20 g) were rendered
858 DKA with a single intraperitoneal injection of 210 mg/kg streptozotocin in 0.2 ml citrate buffer
859 10 days prior to fungal challenge. On days −2 and +3 relative to infection, mice were given a
860 dose of cortisone acetate (250 mg/kg). Diabetic ketoacidotic (DKA) mice were given irradiated
861 food and sterile water containing 50 μg/ml Baytril (Bayer) ad libitum. DKA mice were infected
862 intratracheally with fungal spores with a target inoculum of 2.5×10^5 spores of RNAi-empty
863 plasmid (Control strain) or RNAi-mucoricin (targeting mucoricin gene expression) in 25 μl. To
864 confirm the fidelity of the inoculum, three mice were sacrificed immediately after inoculation,
865 their lungs were homogenized in PBS and quantitatively cultured on PDA plates containing 0.1%
866 triton, and colonies were counted after a 24-hour incubation period at 37°C. Average inhaled
867 inoculum for RNAi-empty plasmid and RNAi-mucoricin were 8.6×10^3 and 3.3×10^3 spores
868 from two experiments, respectively. Primary endpoint was time to moribundity analyzed by
869 Kaplan Meier plots. In another experiment, DKA mice were infected as above and then
870 sacrificed on Day +4 relative to infection, when their lungs and brains (primary and secondary
871 target organs) were collected and processed for determination of tissue fungal burden by qPCR[21].
872 The ability of the IgG anti-toxin to protect against *Rhizopus* infection was also evaluated in the
873 DKA mouse model. Briefly, DKA mice were infected with *R. delemar* 99-880 as above (average
874 inhaled inoculum of 5.6×10^3 spores from two experiments) and 24 h later were injected
875 intraperitoneally with either a 30 μg of IgG anti-toxin or normal rabbit IgG (R & D Systems, Cat
876 # AB-105-C). The survival of mouse and tissue fungal burden of target organs collected on Day
877 +4 post infection served as endpoints as above. Furthermore, histopathological examination was

878 carried out on sections of the organs harvested on Day +4 post infection. These organs were
879 fixed in 10% zinc formalin and processed as above for histological examination with H&E, PAS
880 or Grocott staining.

881 Apoptotic cells in the lung were detected by immunohistochemistry using the ApopTag
882 *in situ* apoptosis detection kit (EMD Millipore) following the manufacturer's directions. Briefly,
883 paraffin-embedded sections were rehydrated in Histo-Clear II (National Diagnostics) and
884 alcohols followed by washing with phosphate-buffered saline (PBS). The sections were pre-
885 treated with 20 μg/ml Proteinase K (Ambion) in PBS for 15 min at room temperature.
886 Endogenous peroxidases were blocked by incubation of the slides for 15 min in 3% hydrogen
887 peroxide. Sections were incubated with equilibration buffer (EMD Millipore) for 30 sec at RT,
888 followed by terminal deoxynucleotidyl transferase (TdT; EMD Millipore) at 37°C for 1 h.
889 Sections were further exposed to anti-Digoxignenin for 30 min at RT, and the positive reaction
890 was visualized with DAB 3, 3-diaminobenzidine (DAB) substrate (Thermo Scientific). After
891 counterstaining the specimens with 0.5% methyl green (Sigma), they were imaged by bright field
892 microscopy. For quantification, apoptotic areas were quantified using PROGRES GRYPHAX®
893 software (Jenoptik).
894

895 **Immunofluorescence staining for mucoricin in human tissue samples.** Paraffin-embedded
896 human lung tissue from a patient diagnosed with disseminated mucormycosis[9] or a patient with
897 proven invasive pulmonary aspergillosis were cut into 5 μm sections that were then mounted
898 onto glass slides. Organ sections on slides were deparaffinized and rehydrated with an ethanol
899 gradient (100%-70%) followed by incubation of the slides in water and heat-induced antigen
900 retrieval in sodium citrate buffer (10 mM, pH 6). Sections were blocked with 3% bovine serum

albumin (BSA) in PBS (BSA-PBS), incubated for 1 h with 1:50 dilution of the IgG anti-mucoricin in PBS, washed twice in PBS, stained with 1:500 dilution of the appropriate goat anti-rabbit IgG Alexa Fluor® 488 (Life Technologies, Cat #A-11034) in 1x PBS, followed by DNA staining with 1 µM TOPRO-3 iodide (642/661; Invitrogen) and staining of the fungal hyphae with 100 µg/ml Fluorescent Brightener 28 (Sigma-Aldrich, Cat #475300). After washing with 1x PBS, slides were mounted in Prolong Gold antifade media (Molecular Probes). Images were acquired using a laser-scanning spectral confocal microscope (TCS SP8; Leica), LCS Lite software (Leica), and a 40× Apochromat 1.25 NA oil objective using identical gain settings. A low fluorescence immersion oil (11513859; Leica) was used, and imaging was performed at room temperature. Serial confocal sections at 0.5 µm steps within a z-stack spanning a total thickness of 10 to 12 µm of tissue, and 3D images were generated using the LCS Lite software. Corresponding tissue sections from the same area were also stained with hematoxylin and eosin.

Statistical analysis. The data was collected and graphed and statistically analyzed using Microsoft Office 360 and Graph Pad 8.0 for Windows or Mac (GraphPad Software, La Jolla, CA, USA). Cell damage and gene expression were analyzed using one-way analysis of variance (ANOVA) using Dunnett's Multiple Comparison Test. The non-parametric log-rank test was used to determine differences in mouse survival times. Differences in tissue fungal burdens were compared by the non-parametric Wilcoxon rank sum test for multiple comparisons. $P < 0.05$ was considered as significant. All *in vitro* experiments were performed at least in triplicate and replicated at least once.

Study approval. All procedures involving mice were approved by the IACUC of The Lundquist Institute for Biomedical Innovations at Harbor-UCLA Medical Center, according to the NIH guidelines for animal housing and care. Human endothelial cell collection was approved by the IRB of The Lundquist Institute for Biomedical Innovations at Harbor-UCLA Medical Center. Because umbilical cords are collected without donor identifiers, the IRB considers them medical waste not subject to informed consent. The purification and testing of ricin were approved by the IRB at UT Southwestern and carried out under BSL3 guidelines. Approval for the collection of tissue samples from the patients with mucormycosis and invasive pulmonary aspergillosis was obtained and the Ethics Committee of the University Hospital of Heraklion, Crete, Greece (5159/2014). The patients provided written informed consent in accordance with the Declaration of Helsinki.

Data availability. Source data are provided with this paper.

References

1 Gleissner, B., Schilling, A., Anagnostopolous, I., Siehl, I. & Thiel, E. Improved outcome of zygomycosis in patients with hematological diseases? *Leuk Lymphoma* **45**, 1351-1360 (2004).

2 Kauffman, C. A. Zygomycosis: reemergence of an old pathogen. *Clin Infect Dis* **39**, 588-590 (2004).

3 Kontoyiannis, D. P., Wessel, V. C., Bodey, G. P. & Rolston, K. V. Zygomycosis in the 1990s in a tertiary-care cancer center. *Clin Infect Dis* **30**, 851-856 (2000).

4 Marr, K. A., Carter, R. A., Crippa, F., Wald, A. & Corey, L. Epidemiology and outcome of mould infections in hematopoietic stem cell transplant recipients. *Clin Infect Dis* **34**, 909-917 (2002).

5 Siwek, G. T. *et al.* Invasive zygomycosis in hematopoietic stem cell transplant recipients receiving voriconazole prophylaxis. *Clin Infect Dis* **39**, 584-587 (2004).

6 Spellberg, B., Edwards Jr., J. & Ibrahim, A. Novel perspectives on mucormycosis: pathophysiology, presentation, and management. *Clin Microbiol Rev* **18**, 556-569 (2005).

7 Neblett Fanfair, R. *et al.* Necrotizing cutaneous mucormycosis after a tornado in Joplin, Missouri, in 2011. *N Engl J Med* **367**, 2214-2225, doi:10.1056/NEJMoa1204781 (2012).

8 Tribble, D. R. & Rodriguez, C. J. Combat-Related Invasive Fungal Wound Infections. *Curr Fungal Infect Rep* **8**, 277-286, doi:10.1007/s12281-014-0205-y (2014).

9 Andrianaki, A. M. *et al.* Iron restriction inside macrophages regulates pulmonary host defense against Rhizopus species. *Nature communications* **9**, 3333-3333, doi:10.1038/s41467-018-05820-2 (2018).

10 Liu, M. *et al.* The endothelial cell receptor GRP78 is required for mucormycosis pathogenesis in diabetic mice. *J Clin Invest* **120**, 1914-1924, doi:42164 [pii]10.1172/JCI42164.

11 Gebremariam, T. *et al.* CotH3 mediates fungal invasion of host cells during mucormycosis. *J Clin Invest* **124**, 237-250, doi:10.1172/JCI71349 (2014).

12 Gebremariam, T. *et al.* Bicarbonate correction of ketoacidosis alters host-pathogen interactions and alleviates mucormycosis. *J Clin Invest*, doi:10.1172/JCI82744 (2016).

13 Ibrahim, A. S., Spellberg, B., Avanessian, V., Fu, Y. & Edwards, J. E., Jr. Rhizopus oryzae adheres to, is phagocytosed by, and damages endothelial cells in vitro. *Infect Immun* **73**, 778-783 (2005).

14 Bozza, W. P., Tolleson, W. H., Rivera Rosado, L. A. & Zhang, B. Ricin detection: Tracking active toxin. *Biotechnology Advances* **33**, 117-123, doi:http://dx.doi.org/10.1016/j.biotechadv.2014.11.012 (2015).

15 Bradshaw, T. *A user's guide: introduction to peptide and protein HPLC*, <http://www.phenomenex.com/lib/4672_Intro2Peptide_Protein_Guide.pdf> (2006).

16 Chibucos, M. C. *et al.* An integrated genomic and transcriptomic survey of mucormycosis-causing fungi. *Nat Commun* **7**, 12218, doi:10.1038/ncomms12218 (2016).

17 Schwartze, V. U. *et al.* Gene expansion shapes genome architecture in the human pathogen Lichtheimia corymbifera: an evolutionary genomics analysis in the ancient terrestrial mucorales (Mucoromycotina). *PLoS Genet* **10**, e1004496, doi:10.1371/journal.pgen.1004496 (2014).

18 Lee, S. C. *et al.* Analysis of a Food-Borne Fungal Pathogen Outbreak: Virulence and Genome of a Mucor circinelloides Isolate from Yogurt. *mBio* **5**, e01390-01314, doi:10.1128/mBio.01390-14 (2014).

19 Ma, L. J. *et al.* Genomic analysis of the basal lineage fungus Rhizopus oryzae reveals a whole-genome duplication. *PLoS Genet* **5**, e1000549, doi:10.1371/journal.pgen.1000549 (2009).

20 Ibrahim, A. S. *et al.* The high affinity iron permease is a key virulence factor required for Rhizopus oryzae pathogenesis. *Mol Microbiol* **77**, 587-604, doi:10.1111/j.1365-2958.2010.07234.x (2010).

21 Luo, G. *et al.* Efficacy of liposomal amphotericin B and posaconazole in intratracheal models of murine mucormycosis. *Antimicrob Agents Chemother* **57**, 3340-3347, doi:10.1128/AAC.00313-13 (2013).

22 Liu, H. *et al.* Functional convergence of gliP and aspf1 in Aspergillus fumigatus pathogenicity. *Virulence* **9**, 1062-1073, doi:10.1080/21505594.2018.1482182 (2018).

23 Medzhitov, R., Schneider, D. S. & Soares, M. P. Disease tolerance as a defense strategy. *Science (New York, N.Y.)* **335**, 936-941, doi:10.1126/science.1214935 (2012).

24 Endo, Y. & Tsurugi, K. RNA N-glycosidase activity of ricin A-chain. Mechanism of action of the toxic lectin ricin on eukaryotic ribosomes. *J Biol Chem* **262**, 8128-8130 (1987).

25 Baluna, R., Rizo, J., Gordon, B. E., Ghetie, V. & Vitetta, E. S. Evidence for a structural motif in toxins and interleukin-2 that may be responsible for binding to endothelial cells and initiating vascular leak syndrome. *Proceedings of the National Academy of Sciences* **96**, 3957-3962, doi:10.1073/pnas.96.7.3957 (1999).

26 Baluna, R., Coleman, E., Jones, C., Ghetie, V. & Vitetta, E. S. The effect of a monoclonal antibody coupled to ricin A chain-derived peptides on endothelial cells in vitro: insights into toxin-mediated vascular damage. *Exp Cell Res* **258**, 417-424, doi:10.1006/excr.2000.4954 (2000).

27 Baluna, R. & Vitetta, E. S. An in vivo model to study immunotoxin-induced vascular leak in human tissue. *J Immunother* **22**, 41-47, doi:10.1097/00002371-199901000-00006 (1999).

28 Earl, R. & D., R. J. Structure of ricin B-chain at 2.5 Å resolution. *Proteins: Structure, Function, and Bioinformatics* **10**, 260-269, doi:doi:10.1002/prot.340100310 (1991).

29 Schrot, J., Weng, A. & Melzig, M. F. Ribosome-inactivating and related proteins. *Toxins* **7**, 1556-1615, doi:10.3390/toxins7051556 (2015).

30 Rong, Y. *et al.* Spatial location of neutralizing and non-neutralizing B cell epitopes on domain 1 of ricin toxin's binding subunit. *PLOS ONE* **12**, e0180999, doi:10.1371/journal.pone.0180999 (2017).

31 Walsh, M. J., Dodd, J. E. & Hautbergue, G. M. Ribosome-inactivating proteins: potent poisons and molecular tools. *Virulence* **4**, 774-784, doi:10.4161/viru.26399 (2013).

32 Becher, F., Duriez, E., Volland, H., Tabet, J. C. & Ezan, E. Detection of Functional Ricin by Immunoaffinity and Liquid Chromatography−Tandem Mass Spectrometry. *Analytical Chemistry* **79**, 659-665, doi:10.1021/ac061498b (2007).

33 Press, O. W., Vitetta, E. S. & Martin, P. J. A simplified microassay for inhibition of protein synthesis in reticulocyte lysates by immunotoxins. *Immunol Lett* **14**, 37-41, doi:10.1016/0165-2478(86)90017-9 (1986).

34 Fulton, R. J. *et al.* Purification of ricin A1, A2, and B chains and characterization of their toxicity. *Journal of Biological Chemistry* **261**, 5314-5319 (1986).

35 Davis, C. T. *et al.* ARF6 inhibition stabilizes the vasculature and enhances survival during endotoxic shock. *J Immunol* **192**, 6045-6052, doi:jimmunol.1400309 [pii]10.4049/jimmunol.1400309.

36 Licastro, F., Morini, M. C., Bolognesi, A. & Stirpe, F. Ricin induces the production of tumour necrosis factor-alpha and interleukin-1 beta by human peripheral-blood mononuclear cells. *Biochem J* **294 (Pt 2)**, 517-520, doi:10.1042/bj2940517 (1993).

37 Korcheva, V. *et al.* Role of apoptotic signaling pathways in regulation of inflammatory responses to ricin in primary murine macrophages. *Mol Immunol* **44**, 2761-2771, doi:10.1016/j.molimm.2006.10.025 (2007).

38 Alaux, P.-L., César, V., Naveau, F., Cranenbrouck, S. & Declerck, S. Impact of Rhizophagus irregularis MUCL 41833 on disease symptoms caused by Phytophthora infestans in potato grown under field conditions. *Crop Protection* **107**, 26-33, doi:https://doi.org/10.1016/j.cropro.2018.01.003 (2018).

39 Wu, X.-C. *et al.* Isolation and partial characterization of antibiotics produced by Paenibacillus elgii B69. *FEMS Microbiology Letters* **310**, 32-38, doi:10.1111/j.1574-6968.2010.02040.x (2010).

40 Sharma, N. *et al.* Isolation and characterization of an RIP (ribosome-inactivating protein)-like protein from tobacco with dual enzymatic activity. *Plant Physiol* **134**, 171-181, doi:10.1104/pp.103.030205 (2004).

41 Parkash, A., Ng, T. B. & Tso, W. W. Isolation and characterization of luffacylin, a ribosome inactivating peptide with anti-fungal activity from sponge gourd (Luffa cylindrica) seeds. *Peptides* **23**, 1019-1024, doi:10.1016/s0196-9781(02)00045-1 (2002).

42 Hovde, C. J., Calderwood, S. B., Mekalanos, J. J. & Collier, R. J. Evidence that glutamic acid 167 is an active-site residue of Shiga-like toxin I. *Proceedings of the National Academy of Sciences* **85**, 2568-2572, doi:10.1073/pnas.85.8.2568 (1988).

43 Basu, D. *et al.* The A1 Subunit of Shiga Toxin 2 Has Higher Affinity for Ribosomes and Higher Catalytic Activity than the A1 Subunit of Shiga Toxin 1. *Infect Immun* **84**, 149-161, doi:10.1128/iai.00994-15 (2016).

44 Jackson, M. P., Deresiewicz, R. L. & Calderwood, S. B. Mutational analysis of the Shiga toxin and Shiga-like toxin II enzymatic subunits. *J Bacteriol* **172**, 3346-3350, doi:10.1128/jb.172.6.3346-3350.1990 (1990).

45 Polito, L., Bortolotti, M., Mercatelli, D., Battelli, M. G. & Bolognesi, A. Saporin-S6: a useful tool in cancer therapy. *Toxins* **5**, 1698-1722, doi:10.3390/toxins5101698 (2013).

46 Narayanan, S., Surendranath, K., Bora, N., Surolia, A. & Karande, A. A. Ribosome inactivating proteins and apoptosis. *FEBS Letters* **579**, 1324-1331, doi:https://doi.org/10.1016/j.febslet.2005.01.038 (2005).

47 Watkins, T. N. *et al.* Inhibition of EGFR Signaling Protects from Mucormycosis. *mBio* **9**, e01384-01318, doi:10.1128/mBio.01384-18 (2018).

48 Alqarihi, A. *et al.* GRP78 and Integrins Play Different Roles in Host Cell Invasion during Mucormycosis. *mBio* **11**, e01087-01020, doi:10.1128/mBio.01087-20 (2020).

49 Gonzalez, T. V., Farrant, S. A. & Mantis, N. J. Ricin induces IL-8 secretion from human monocyte/macrophages by activating the p38 MAP kinase pathway. *Mol Immunol* **43**, 1920-1923, doi:10.1016/j.molimm.2005.11.002 (2006).

50 Lindauer, M. L., Wong, J., Iwakura, Y. & Magun, B. E. Pulmonary inflammation triggered by ricin toxin requires macrophages and IL-1 signaling. *J Immunol* **183**, 1419-1426, doi:10.4049/jimmunol.0901119 (2009).

51 Yoder, J. M., Aslam, R. U. & Mantis, N. J. Evidence for widespread epithelial damage and coincident production of monocyte chemotactic protein 1 in a murine model of intestinal ricin intoxication. *Infect Immun* **75**, 1745-1750, doi:10.1128/IAI.01528-06 (2007).

52 Lee, S. C., Li, A., Calo, S. & Heitman, J. Calcineurin Plays Key Roles in the Dimorphic Transition and Virulence of the Human Pathogenic Zygomycete Mucor circinelloides. *PLOS Pathogens* **9**, e1003625, doi:10.1371/journal.ppat.1003625 (2013).

53 Lee, S. C. *et al.* Calcineurin orchestrates dimorphic transitions, antifungal drug responses and host-pathogen interactions of the pathogenic mucoralean fungus Mucor circinelloides. *Mol Microbiol* **97**, 844-865, doi:10.1111/mmi.13071 (2015).

54 Spellberg, B. *et al.* The Deferasirox-AmBisome Therapy for Mucormycosis (DEFEAT Mucor) study: a randomized, double-blinded, placebo-controlled trial. *J Antimicrob Chemother* **67**, 715-722, doi:dkr375 [pii]10.1093/jac/dkr375.

55 Skory, C. D. & Ibrahim, A. S. Native and modified lactate dehydrogenase expression in a fumaric acid producing isolate Rhizopus oryzae 99-880. *Curr Genet* **52**, 23-33, doi:10.1007/s00294-007-0135-0 (2007).

56 Jaffe, E. A., Nachman, R. L., Becker, C. G. & Minick, C. R. Culture of human endothelial cells derived from umbilical veins. Identification by morphologic and immunologic criteria. *J Clin Invest* **52**, 2745-2756 (1973).

57 Farowski, F. *et al.* Quantitation of azoles and echinocandins in compartments of peripheral blood by liquid chromatography-tandem mass spectrometry. *Antimicrobial agents and chemotherapy* **54**, 1815-1819, doi:10.1128/AAC.01276-09 (2010).

58 Simmons, B. M. & Russell, J. H. A single affinity column step method for the purification of ricin toxin from castor beans (Ricinus communis). *Analytical Biochemistry* **146**, 206-210, doi:https://doi.org/10.1016/0003-2697(85)90417-8 (1985).

59 Press, O. W., Vitetta, E. S. & Martin, P. J. A simplified microassay for inhibition of protein synthesis in reticulocyte lysates by immunotoxins. *Immunology Letters* **14**, 37-41, doi:https://doi.org/10.1016/0165-2478(86)90017-9 (1986).

60 Bertoni, M., Kiefer, F., Biasini, M., Bordoli, L. & Schwede, T. Modeling protein quaternary structure of homo- and hetero-oligomers beyond binary interactions by homology. *Scientific reports* **7**, 10480-10480, doi:10.1038/s41598-017-09654-8 (2017).

61 Guex, N., Peitsch, M. C. & Schwede, T. Automated comparative protein structure modeling with SWISS-MODEL and Swiss-PdbViewer: a historical perspective. *Electrophoresis* **30 Suppl 1**, S162-173, doi:10.1002/elps.200900140 (2009).

62 Waterhouse, A. *et al.* SWISS-MODEL: homology modelling of protein structures and complexes. *Nucleic Acids Res* **46**, W296-W303, doi:10.1093/nar/gky427 (2018).

63 Zhang, Y. & Skolnick, J. TM-align: a protein structure alignment algorithm based on the TM-score. *Nucleic Acids Res* **33**, 2302-2309, doi:10.1093/nar/gki524 (2005).

64 Fu, Y. *et al.* Cloning and functional characterization of the Rhizopus oryzae high affinity iron permease (rFTR1) gene. *FEMS Microbiol Lett* **235**, 169-176, doi:10.1016/j.femsle.2004.04.031S0378109704002903 [pii] (2004).

65 Zabala, A. O., Chooi, Y.-H., Choi, M. S., Lin, H.-C. & Tang, Y. Fungal polyketide synthase product chain-length control by partnering thiohydrolase. *ACS chemical biology* **9**, 1576-1586, doi:10.1021/cb500284t (2014).

66 Malyala, P. & Singh, M. Endotoxin limits in formulations for preclinical research. *J Pharm Sci* **97**, 2041-2044, doi:10.1002/jps.21152 (2008).

67 Ibrahim, A. S. *et al.* Bacterial endosymbiosis is widely present among zygomycetes but does not contribute to the pathogenesis of mucormycosis. *J Infect Dis* **198**, 1083-1090, doi:10.1086/591461 (2008).

68 Ghannoum, M. A., Filler, S. G., Ibrahim, A. S., Fu, Y. & Edwards, J. E., Jr. Modulation of interactions of Candida albicans and endothelial cells by fluconazole and amphotericin B. *Antimicrobial agents and chemotherapy* **36**, 2239-2244, doi:10.1128/aac.36.10.2239 (1992).

69 Caillot, D. *et al.* Is It Time to Include CT "Reverse Halo Sign" and qPCR Targeting Mucorales in Serum to EORTC-MSG Criteria for the Diagnosis of Pulmonary Mucormycosis in Leukemia Patients? *Open Forum Infect Dis* **3**, ofw190, doi:10.1093/ofid/ofw190 (2016).

70 Liu, M. *et al.* Fob1 and Fob2 Proteins Are Virulence Determinants of Rhizopus oryzae via Facilitating Iron Uptake from Ferrioxamine. *PLoS Pathog* **11**, e1004842, doi:10.1371/journal.ppat.1004842 (2015).

71 Pfaffl, M. W. A new mathematical model for relative quantification in real-time RT-PCR. *Nucleic Acids Res* **29**, e45 (2001).

72 Livak, K. J. & Schmittgen, T. D. Analysis of relative gene expression data using real-time quantitative PCR and the 2(-Delta Delta C(T)) Method. *Methods* **25**, 402-408, doi:10.1006/meth.2001.1262S1046-2023(01)91262-9 [pii] (2001).

73 OSBORN, R. W. & HARTLEY, M. R. Dual effects of the ricin A chain on protein synthesis in rabbit reticulocyte lysate. *European Journal of Biochemistry* **193**, 401-407, doi:10.1111/j.1432-1033.1990.tb19353.x (1990).

74 Tumer, N. E., Hwang, D. J. & Bonness, M. C-terminal deletion mutant of pokeweed antiviral protein inhibits viral infection but does not depurinate host ribosomes. *Proceedings of the National Academy of Sciences of the United States of America* **94**, 3866-3871, doi:10.1073/pnas.94.8.3866 (1997).

75 Gebremariam, T. *et al.* Preserving Vascular Integrity Protects Mice Against Multidrug-Resistant Gram-Negative Bacterial Infection. *Antimicrobial Agents and Chemotherapy*, AAC.00303-00320, doi:10.1128/aac.00303-20 (2020).

76 Sheppard, D. C. *et al.* Novel inhalational murine model of invasive pulmonary aspergillosis. *Antimicrob Agents Chemother* **48**, 1908-1911 (2004).

77 Kap, M. *et al.* Histological assessment of PAXgene tissue fixation and stabilization reagents. *PloS one* **6**, e27704-e27704, doi:10.1371/journal.pone.0027704 (2011).

78 Mertens, J. A., Skory, C. D. & Ibrahim, A. S. Plasmids for expression of heterologous proteins in Rhizopus oryzae. *Arch Microbiol* **186**, 41-50 (2006).

79 Gebremariam, T. *et al.* Anti-CotH3 antibodies protect mice from mucormycosis by prevention of invasion and augmenting opsonophagocytosis. *Science Advances* **5**, eaaw1327, doi:10.1126/sciadv.aaw1327 (2019).

Figure Legends

Figure 1. *R. delemar* toxin is sufficient to cause damage *in vitro* and *in vivo.* (**a**) The effect of toxin on different cell lines (n=7 wells /time point pooled from three independent experiments). Data are median ± interquartile range. Statistical analysis was performed by using the non-parametric Mann-Whitney (two-tailed) test comparing HUVECs *vs.* primary alveolar epithelial cells or A549 alveolar cells. **(b)** Damage of extracted or recombinant toxin (~ 500 μg/ml or 29.4 μM) on epithelial cells at different time points (n=3 wells/time point). Data are representative of three independent experiments and presented as median ± interquartile range. (**c**) Mouse (n=3 mice/group) weight loss (data are median ± interquartile range) and **(d**) percent survival (n=3 mice/group) following intravenous injection with 0.1 mg/ml (5.9 μM) toxin QOD x 3. **(e**) Mouse organ H&E histomicrographs showing the effects of the toxin. Livers showed necrosis (white arrow), infiltration and calcification of PMNs (black arrow) due to inflammation and a cluster of mononuclear cells (cyan arrow). Lungs showed megakaryocytes (black arrow) and hemorrhage (yellow arrow). Data in each group are representative of 2 mice. Scale bar 50 μm for first liver micrograph and 100 μm for all other. For lung micrographs scale bar 50 μm.

Figure 2. Inhibition of *R. delemar* toxin attenuates virulence of *R. delemar.* (a) RNAi toxin shows reduced damage to A549 cells compared to wild type or empty plasmid *R. delamar* (n=6 wells/group pooled from three independent experiments). Data are median ± interquartile range. Statistical comparisons are by the non-parametric Mann-Whitney (two-tailed) test. (**b**) IgG anti-toxin antibodies reduced *R. delemar*-induced injury of A549 cells compared to *R. delamar* without IgG or normal rabbit IgG (n = 13 wells/group pooled from three independent experiments). Data are median ± interquartile range. Statistical comparisons are by the non-parametric Mann-Whitney (two-tailed) test. **(c)** RNAi toxin inhibition prolonged survival of mice (n= 18 mice) compared to

R. delamar with empty plasmid (n= 17 mice). Data were pooled from two independent experiments. Survival data were analyzed by Log-rank (Mantel-Cox) test. **(d)** IgG anti-toxin prolonged survival of mice compared to normal rabbit IgG (n=20 mice/group). Data were pooled from two independent experiments. Survival data were analyzed by Log-rank (Mantel-Cox) test. **(e)** Histopathological sections of lungs from uninfected mice, **(f)** mice infected with the RNAi empty plasmid *R. delemar* strain showed hyphae and granulocyte infiltration (left panel, arrows) and angioinvasion (right panel, arrow), *vs.* (**g**) mild signs of inflammation and no angioinvasion for mice infected with RNAi toxin. (**h**) IgG anti-toxin group had normal lung tissue architecture. Data in **e-h** are representative of 3 mice and scale bar is 20 μm.

Figure 3. *R. delemar* toxin and ricin share structural features. (a) *R. delemar* toxin has 29% amino acid sequence identity with ricin. Both toxins share similar motifs and molecular functions. (**b)** 3-D structure model of *R. delemar* toxin shows similarities to ricin B chain. Protein 3D structure models of *R. delamar* toxin and ricin chain B (amino acids 304-437, and 338-565) were aligned residue-to-residue based on structural similarity using heuristic dynamic programming iterations and sequence independent TM-align score (0-1) were calculated based on structural similarity. TM-align score >0.5 considered significant similarity. **(c)** IgG anti-*R. delemar* toxin binds to ELISA plates coated with either *R. delemar* toxin or ricin. (**d**) Ricin is recognized on a dot blot by IgG anti-*R. delemar* toxin. (**e**) Western blot of *R. delemar* toxin and ricin using IgG anti-*R. delemar* toxin IgG. (**f)** IgG anti-*R. delemar* toxin, IgG anti-ricin (8A1 clone) (10 μg/ml each) or galactose (10 mM) inhibit ricin (77 nM)-mediated A549 cell damage (n=9 wells for normal rabbit IgG and Anti-ricin toxin B chain (8A1) group, n=8 for IgG anti-*R. delemar* toxin and galactose group pooled from three independent experiments). Data are median ± interquartile

range. Statistical comparisons were made by using the non-parametric Mann-Whitney (two-tailed) test.

Figure 4. *R. delemar* toxin and ricin have functional similarities. (a,b) Cell-free rabbit reticulocyte assay showing protein synthesis inhibition by ricin (IC_{50} of 2.2 x 10^{-11} M) **(a)** and *R. delemar* toxin (IC_{50} of 1.7 x 10^{-8} M) **(b)**. Data (n=7 wells/concentrations for ricin; and n=6 wells/concentration for *R. delemar* toxin, pooled from three experiments) are presented as median ± interquartile range. **(c)** Representative HPLC chromatograms demonstrating the depurination activity of *R. delemar* toxin of A549 RNA at 3.6 min similar to adenine standard. (**d**) A representative gel (from three experiments) showing rRNA glycosidase activity of *R. delemar* toxin (1 μM) compared to ricin (1 nM) and control OVA (1 nM or 1 μM). Ribosomes were treated with ricin for 1 h or *R. delemar* toxin for 4 h. Extracted RNA were treated with (+) or without (-) aniline prior to running the gel. Arrows point to endo fragment at ~500 bp. (**e, f**) *R. delemar* induces HUVEC permeability via its toxin. *R. delemar* (**e**) or recombinant toxin (2.9 μM) (**f**) were incubated with HUVEC for 5 h with or without 50 μg/ml of IgG isotype-matched or anti-*R. delemar* toxin or 10 μg/ml of IgG anti-ricin chain B (clone 8A1). LPS or OVA were added as a positive and negative controls, respectively. For **e,** n= 13 wells except for IgG anti-ricin 8A1 which n=12 wells pooled from three independent experiments. For **f** , n= 6 wells for Ova, n=10 wells for *R. delamar* toxin alone and *R. delamar* toxin + IgG anti-*R. delmar* toxin, n=11 wells for *R. delamar* toxin + Isotype IgG, n=12 wells for *R. delamar* toxin +IgG anti-ricin (8A1), and n=13 wells for HUVECs and LPS. Data in **e** and **f** were pooled from three independent experiments and presented as median ± interquartile range. (**g**) Detection of apoptosis/necrosis of A549 cells incubated for 2 h with 50 μg/ml (2.9 μM) of *R. delemar* toxin or 5 μg/ml (77 nM) ricin. Apoptotic cells (closed triangle) were identified by green fluorescence while necrotic cells (open triangle) are shown in

1228 red. Scale bar is 50 µm. (**h**) The number of apoptotic and necrotic events per high-power field
1229 (HPF) was determined, counting 10 HPF per coverslip. The data is combined from 3 independent
1230 experiments with each group in triplicate (total n=9 wells) and presented as median ± interquartile
1231 range. Kruskal-wallis test was used to compare control *vs. R. delamar* toxin or ricin.

Extended Data Figures Legends

Extended Data Figure 1. A heat stable and hyphae-associated Mucorales extract damages mammalian host cells *in vitro*. (a) *R. delemar* caused time dependent alveolar epithelial cell damage (n=9 wells/time point, pooled from three independent experiments). Data are median ± interquartile range. **(b)** Heat-killed *R. delemar* hyphae showed ~50% damage to mammalian cells compared to ~100% damage caused by living hyphae (n=6 wells/group, pooled from three independent experiments). Data are median ± interquartile range. Statistical analysis was performed by using Mann-Whitney non-parametric (two-tailed) test comparing live vs killed hyphae. **(c)** Extracts from comparable wet weight of *R. delemar* hyphae/spores, or hyphae, but not spores, damaged alveolar epithelial cells (n=6 wells/group, pooled from three independent experiments). Data are median ± interquartile range. Statistical analysis was performed by using Mann-Whitney non-parametric (two-tailed) test comparing spores vs spore/hyphae or hyphae. **(d)** Disrupted pellet from Mucorales germlings containing the cell-associated fraction was compared to live or heat-killed cells in causing injury to HUVECs (n= 3 wells/group, pooled from three independent experiments). Data are median ± interquartile range. **(e)** Fungal hyphae from representative clinical Mucorales isolates ground in liquid nitrogen and extracted with mammalian cell culture caused significant A549 alveolar epithelial cell damage (n= 3 wells/Mucorales, pooled from three independent experiments). Data are median ± interquartile range. **(f)** IgG anti-*R. delemar* toxin but not normal rabbit IgG (50 μg/ml) blocked host cell damage caused by heat-killed hyphae from different Mucorales (n=8 or 9 replicates/treatment/Mucorales, pooled from three independent experiments). Data presented as median ± interquartile range. Statistical analysis was performed by Mann-Whitney non-parametric (two-tailed) test comparing IgG anti-toxin *vs.* without IgG or normal rabbit IgG.

Extended Data Figure 2. Fractionation and purification of *R. delemar* toxin. (a) Size exclusion of hyphae extracts indicating a 10-30 kDa fraction causing A549 cell damage (n=6 wells/fraction, pooled from three independent experiments). Data are median ± interquartile range. **(b)** Native polyacrylamide fractionation of hyphae extract and **(c)** its corresponding A549 cell damage, showing fraction # 6 causing injury. (n=6 wells/fraction, pooled from three independent experiments). Data are median ± interquartile range. **(d)** Cellulose plate separation of fraction # 6 purified from the polyacrylamide gel and **(e)** its corresponding A 549 cell damage, showing a high polar fraction #6 causing injury. Data are n=6 wells/fraction, and pooled from three independent experiments. Data are median ± interquartile range. **(f)** Third dimension fractionation of the previous fraction # 6 on cellulose plates and **(g)** its corresponding A549 cell injury (n=6 wells/fraction, pooled from three independent experiments). Data are median ± interquartile range.

Extended Data Figure 3. IgG anti-toxin had no effect on growth or germination of *R. delemar*. **(a)** Fungal spores (10^4/ml) were inoculated in 96-well plates with or without 50 μg/ml IgG anti-toxin or normal rabbit IgG for 6 h prior to measuring absorbance at 450 nm. (n=12 wells, data pooled from three independent experiments) Data presented as median + interquartile range. Statistical analysis was performed by Mann-Whitney non-parametric (two-tailed). (**b**) *R. delemar* spores (10^4/ml) were germinated at 37^{o}C for 6 h prior to measuring the germ tube length using light microscopy equipped with a micometer lens. Each data point represents 20-50 germ tubes/HPF. (n=12 wells, data pooled from three independent experiments) Data presented as median + interquartile range from three experiments. Statistical analysis was performed by Mann-Whitney non-parametric (two-tailed).

Extended Data Figure 4. Putative toxin gene expression is cell-, time- and oxygen-dependent. **(a)** Toxin gene expression in *R. delemar* germinating cells in YPD medium. Data (n=3 wells/timepoint, pooled from three independent experiments) are presented as median ± interquartile range. Statistical analysis was performed by using unpaired t-test (two-tailed). **(b)** Confocal imaging of Alexa Flour 488-labelled IgG anti-toxin (green) during the growth of *R. delemar* from spores to hyphae. Scale bar is 50 µm. **(c)** Toxin gene expression from *R. delemar* hyphae grown in YPD culture in sufficient versus limited oxygen (n=6 wells, data pooled from three independent experiments). Data presented as median ± interquartile range. Statistical analysis was performed by using unpaired t-test (two-tailed). **(d)** Toxin gene expression analysis of fungal germlings on different cell types showed a time dependent expression on alveolar epithelial cells compared to HUVECs and erythrocytes (n=3 wells/group, pooled from three independent experiments). Data presented as median ± interquartile range. Statistical analysis was performed by using unpaired t-test (two-tailed).

Extended Data Figure 5. RNAi targeting the putative *R. delemar* toxin inhibits its expression. **(a)** *R. delemar* spores were transformed with RNAi plasmids targeting the putative toxin (RNAi-toxin) or empty plasmid (Empty-plasmid) using biolistic delivery system. Cells were grown in minimal medium without uracil for 24 h prior to extracting RNA (n=6/group, pooled from three independent experiments). Data presented as median ± interquartile range. Statistical analysis was performed by using Mann-Whitney non-parametric (two-tailed) test comparing RNAi- *R. delemar* toxin vs wild-type or empty plasmid **(b)** Representative Western blot and densitometry analyses of the wild-type, empty plasmid, or RNAi toxin strains (n=4 pictures data pooled from four

independent experiments) Data presented as median ± interquartile range. Statistical analysis was performed by using Mann-Whitney non-parametric (two-tailed) test comparing RNAi- *R. delemar* toxin *vs.* wild-type or empty plasmid. **(c)** confocal images showing reduced expression of the toxin in the RNAi toxin mutant. Scale bar is 50 μm.

Extended Data Figure 6. Down regulation of *R. delemar* toxin by RNAi did not affect germination or the growth of the fungus. (a) Wild-type *R. delemar,* RNAi empty plasmid, or RNAi toxin strains were germinated in minimal medium without uracil at 37ºC with shaking. At times, samples were taken from the medium and examined by light microscopy. Scale bar is 5 μm. (**b**) 10^5 spores of wild-type *R. delemar,* RNAi empty plasmid, or RNAi toxin strains were plated in the middle of the minimal medium without uracil agar plates for several days at 37ºC and the colony diameter measured (n=6 plates/group, pooled from three independent experiments). Data are presented as median ± interquartile range.

Extended Data Figure 7. Effect of blocking the expression or the function of *R. delemar* toxin on fungal burdens in mice. (a) Inhibition of the toxin by RNAi did not affect the fungal burden in the lungs or brain of mice harvested on Day +4 post infection (average inoculum from two experiments of 1.4 x 10^4 for empty plasmid [n=22 mice] *vs.* 1.3 x 10^4 for RNAi toxin mutants [n=20 mice]). Data are pooled from two independent experiments and presented as median ± interquartile range. Statistical analysis was performed by using Mann-Whitney non-parametric (two-tailed) test comparing RNAi-*R.delemar* toxin *vs.* Empty plasmid. **(b)** The IgG anti-*R. delemar* toxin had no effect on the fungal burden of lungs or brains of DKA mice harvested on Day +4 post intratracheal infection with wild-type *R. delemar* (average inhaled inoculum of 5.6 x

10^3 spores from two experiments [n=20 mice]). Data are pooled from two independent experiments and presented as median ± interquartile range). Statistical analysis was performed by using Mann-Whitney non-parametric (two-tailed) test comparing IgG anti-*R.delemar* toxin *vs.* normal rabbit IgG.

Extended Data Figure 8. Histology of organs showing involvement of the toxin in tissue damage. (a) Damaged lung tissues (brown color) of mice infected with *R. delemar* transformed with RNAi empty plasmid (n=31 field counts) or RNAi toxin. Statistical analysis was performed by using Mann-Whitney non-parametric (two-tailed) test. Scale bar is 200 µm. (**b**) Damaged lung tissues from mice infected with wild-type *R. delemar* and treated with either normal rabbit IgG (n= 18 field counts) or IgG anti-toxin (n= 18 field counts) were quantified by ApopTag kit. Data were pooled from two independent experiments, are presented as median + interquartile range. Statistical analysis was performed by using Mann-Whitney non-parametric (two-tailed) test. Scale bar is 200 µm.

Extended Data Figure 9. *R. delemar* toxin is expressed in lung tissue collected from a mucormycosis patient but not in lung samples from an aspergillosis patient. H&E staining of lung tissues from mucormycosis **(a)** or aspergillosis **(b)** patients showing broad aseptate hyphae with angioinvasion (Mucorales) and thinner septated hyphae of *Aspergillus.* Scale bar is 10 µm. Box magnification 1400 X. Staining of a mucormycosis **(c)** or aspergillosis **(d)** patient lungs using IgG anti-toxin (green color). Mucorales or *Aspergillus* hyphae are shown in yellow (stained with calcofluor white) and nuclei are shown in magenta. *R. delemar* toxin staining is shown in

association with hyphae (grey arrow) and released in the tissue (white arrow). Scale bar is 10 μm in all micrographs.

Extended Data Figure 10. Secretion/shedding of *R. delemar* toxin in culture supernatant of growth media. (a) Cell-free culture supernatants were collected from *R. delemar* hyphae grown in the presence or absence of 2-fold dilutions of amphotericin B. The XTT assay was used to determine growth of *R. delemar* (left axis, blue bar, n=8 wells/amphotericin B concentration), while toxin release assayed by sandwich ELISA using anti-*R. delemar* mouse monoclonal IgG1 as the capture antibody and rabbit anti-*R. delemar* toxin IgG as the detector antibody (right axis, red bar, n=2 wells/amphotericin B concentration). Data in are representative of three independent experiments and presented as mean ± SD. **(b)** The released toxin concentration from *R. delemar* wild-type, *R. delemar* transformed with empty plasmid RNAi or *R. delemar* with RNAi-toxin was extrapolated from a standard curve using recombinant toxin in the same ELISA assay. Toxin concentrations (n= 3 samples from three independent experiments tested in duplicate in ELISA for each strain) are presented as mean ± SD.

Supplementary Figure Legends

Supplementary Figure 1. Incubation of lower inoculum of *R. delemar* with HUVECs induces minimal to no host cell injury. Data are presented as % ^{51}Cr-released from HUVECs challenged with 1 x 10^5 spores of *R. delemar* for 5 hours after subtracting the amount of ^{51}Cr-released from HUVECs without *R. delemar* challenge. (n= 10 data pooled from three independent experiments). Data presented as median + interquartile range.

Supplementary Figure 2. CLUSTAL multiple sequence alignment by MUSCLE (3.8) between mucoricin and saporin from *Saponaria officinalis.* The predicted Type 1 RIP domain in saporin (shown in yellow) aligned with sequence from mucoricin with 10 out of 17 amino acid residues conserved.

Supplementary Table 1: Results of BLAST search of a ricin-like toxin gene from *R. delemar* 99-880.

Supplementary Table 2. Ten proteins that are structurally similar to mucoricin. The 3-D model of mucoricin was used to identify structurally similar proteins in the protein data bank (PDB) by Tm align.

Supplementary Table 3: Ricin orthologues in different Mucorales and the presence of vascular leak and RIP motifs.

Figure 1

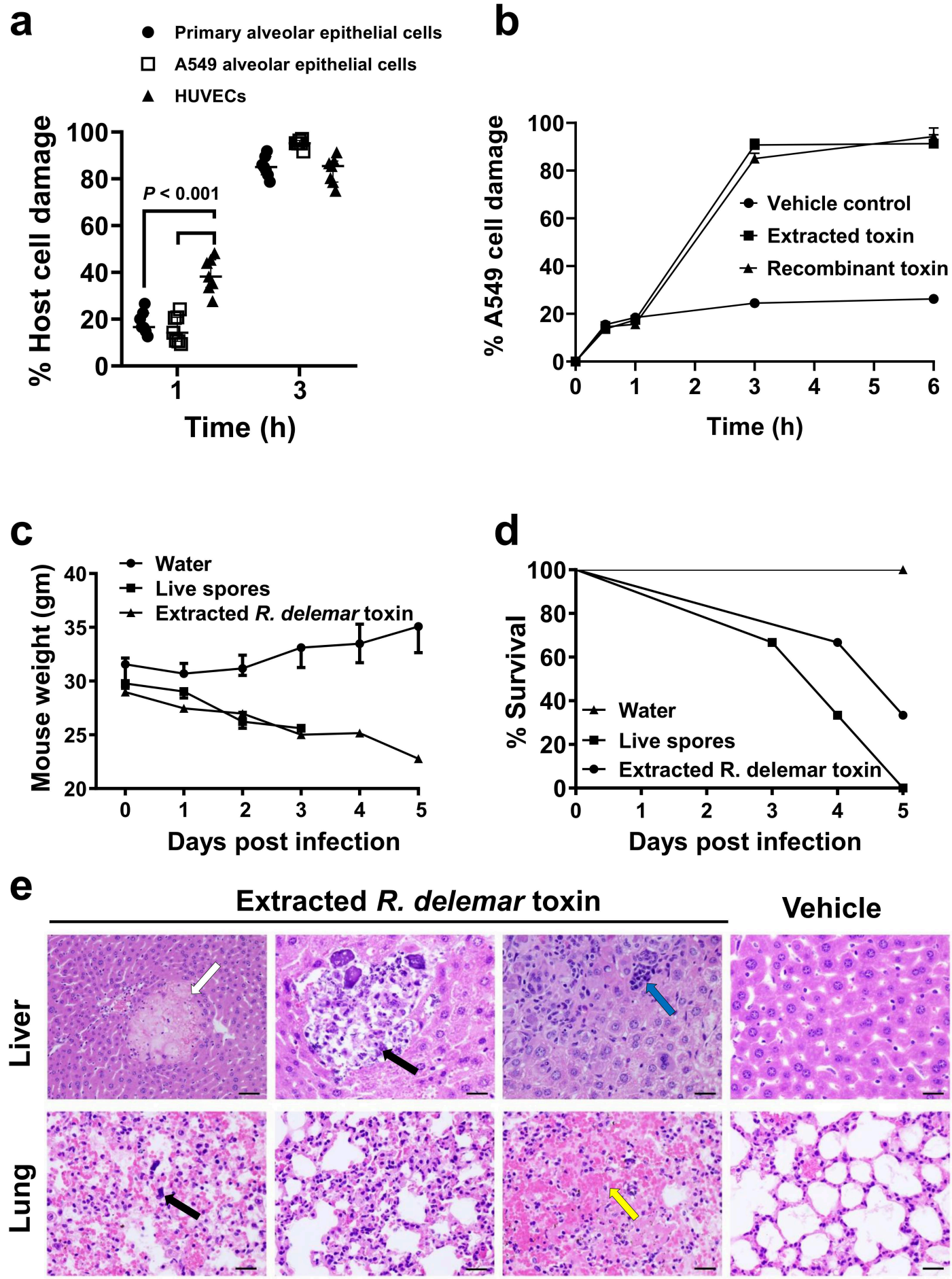

Figure 2

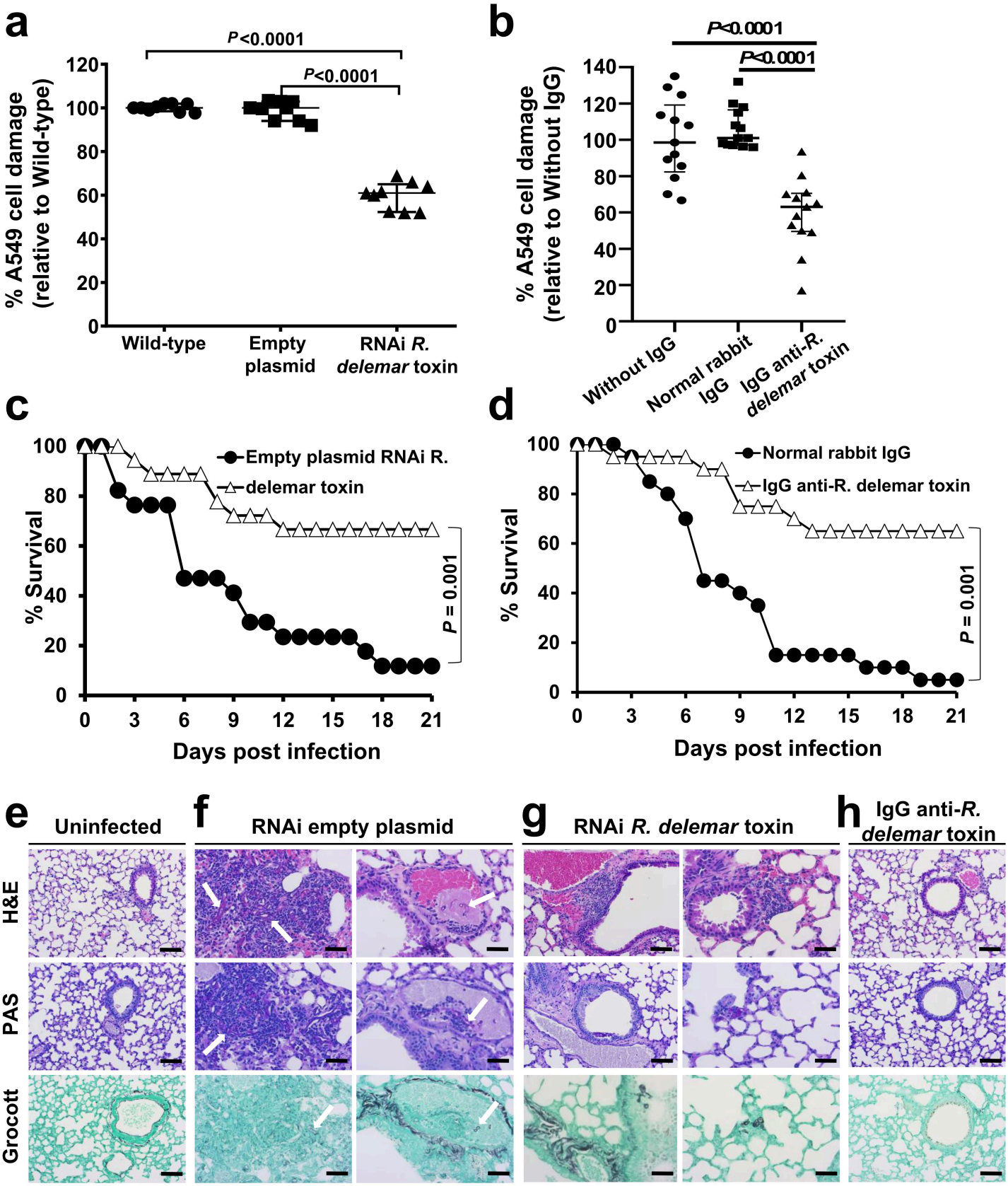

a

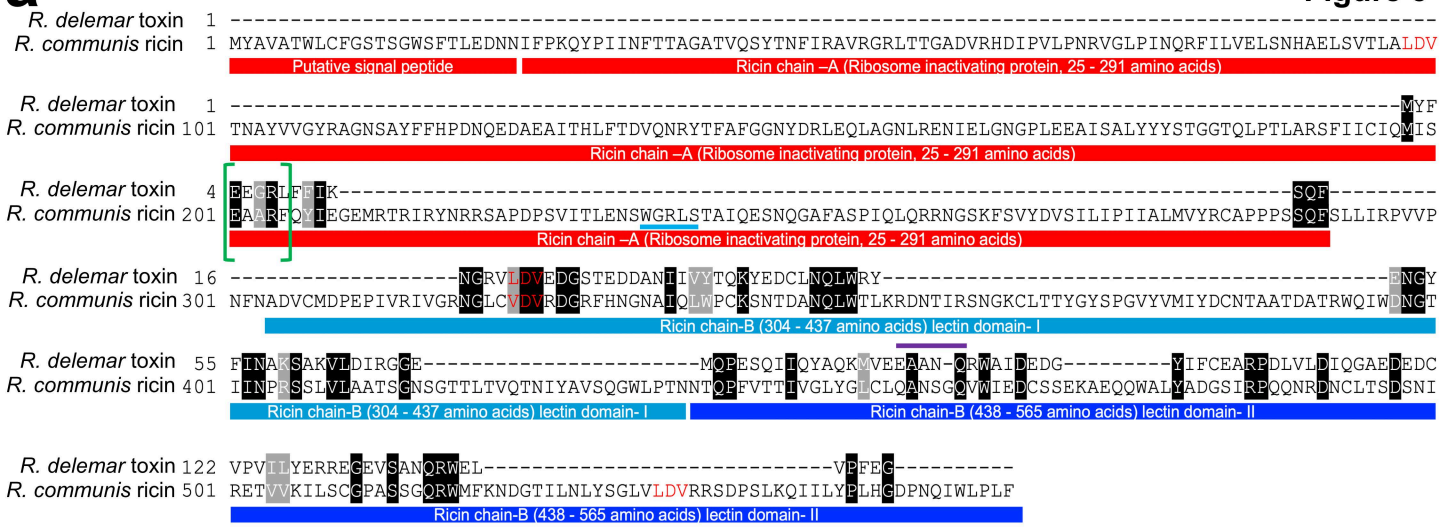

NCBI Sequence ID	Name	Protein sequence homology					Vascular leak motif (LDV/ VDV)	Predicted molecular functions			
		Length	Max Score	Total Score	Query Cover	Identity		Sugar Binding	Lectin Receptor Binding	rRNA N-glycosylase activity	Hydrolase activity
NP_001310630.1	Ricin precursor [*R. communis*]	565	26.6	105	87%	29%	Yes	Yes	Yes	Yes	Yes
EIE81863.1	*R. delemar* toxin	147					Yes	Yes	Yes	Yes	Yes

b

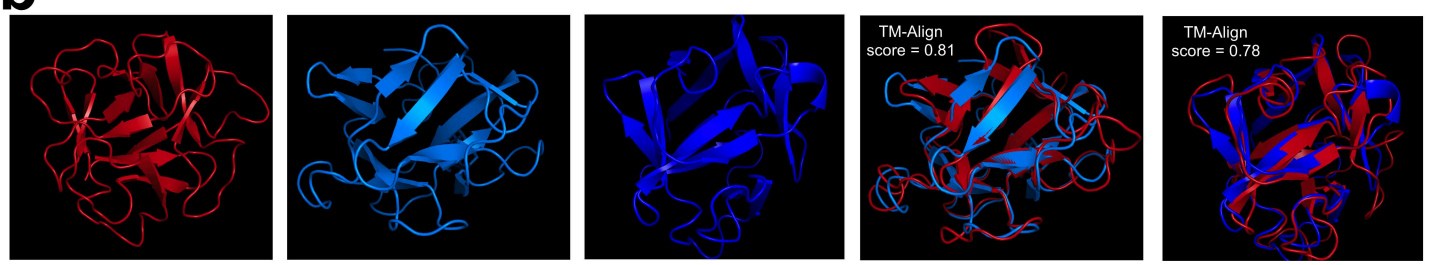

R. delemar toxin | Ricin B chain (304-437 a.a.) | Ricin B chain (438-565 a.a.) | Superimposed (*R. delemar* toxin vs Ricin B chain [304-437 a.a.]) | Superimposed (*R. delemar* toxin vs Ricin B chain [438-565 a.a.])

c

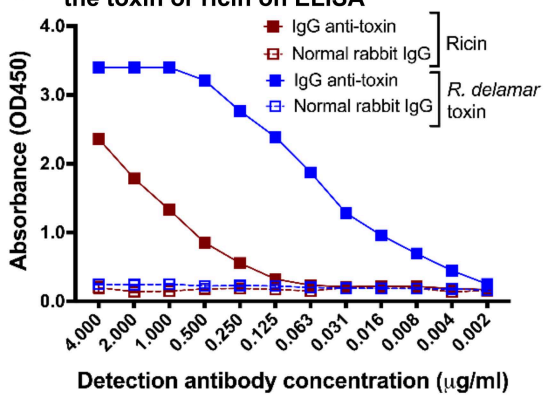

d

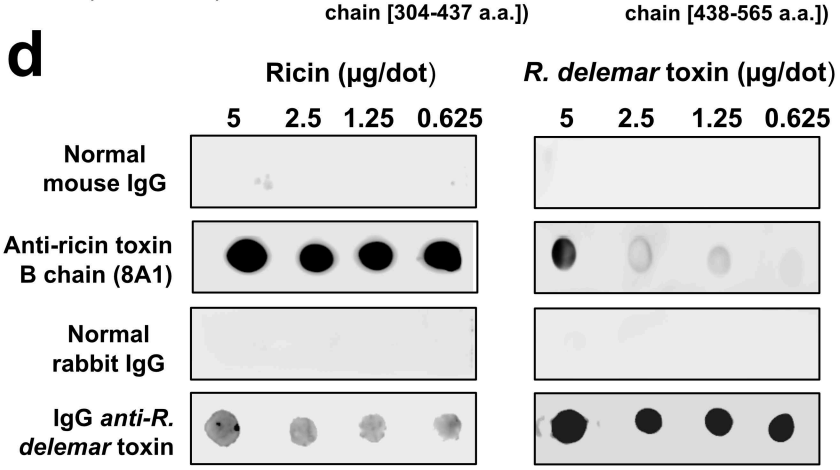

e

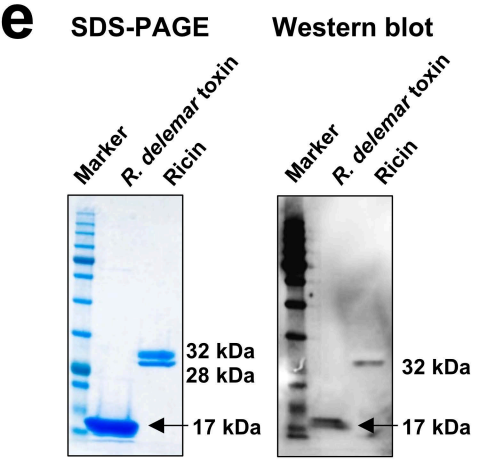

f

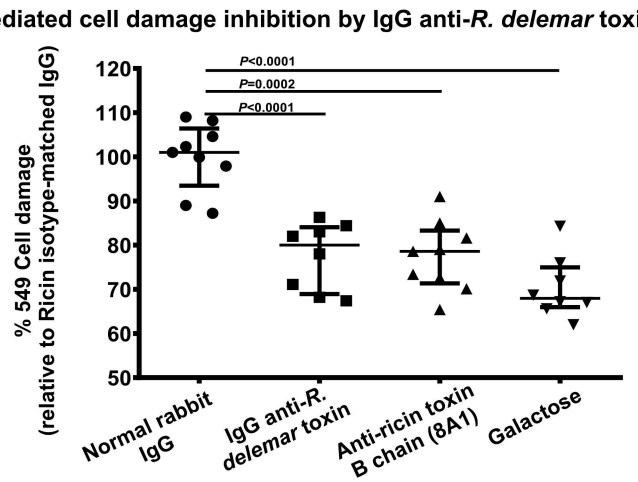

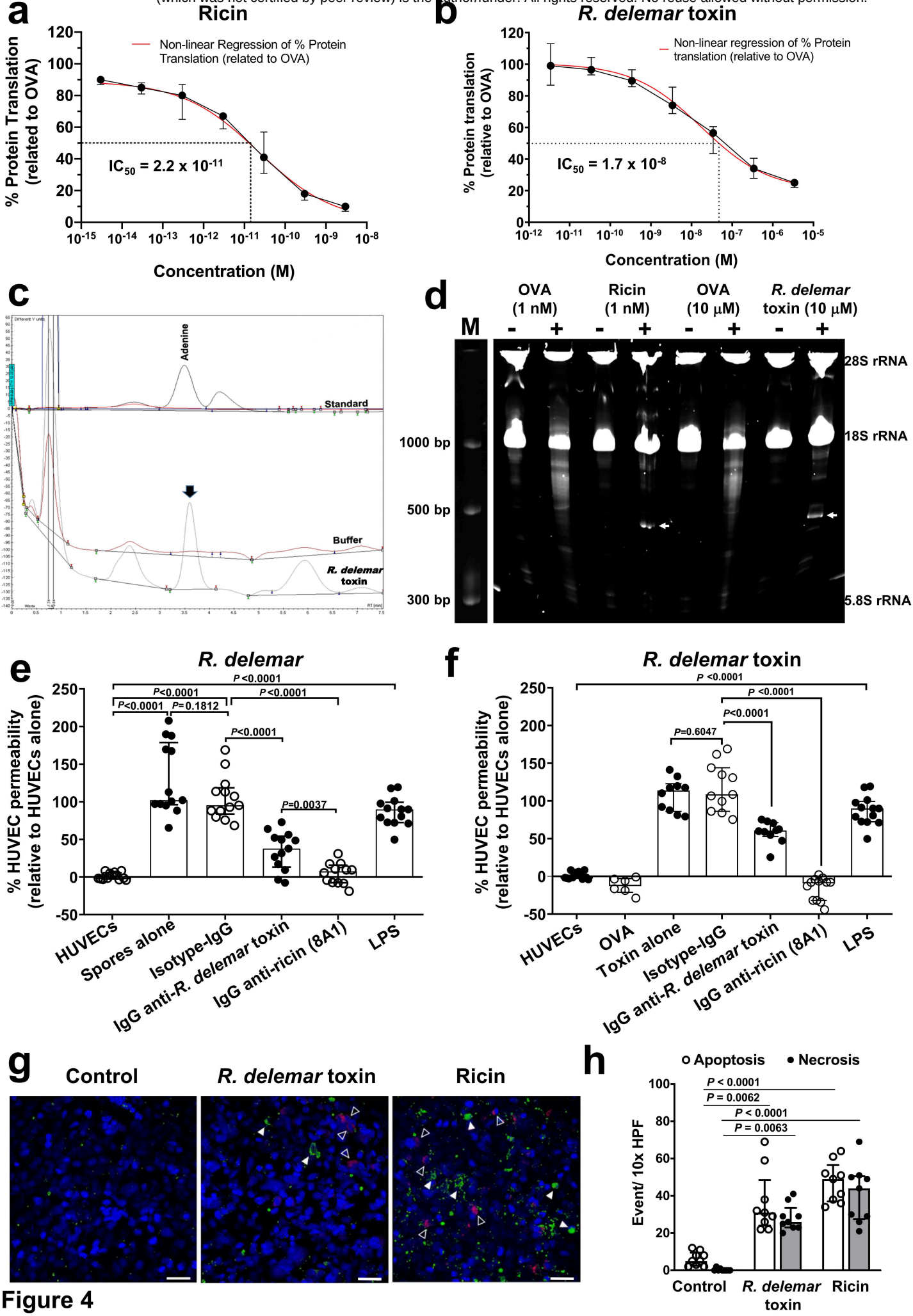

Figure 4

Extended Data Figure 1

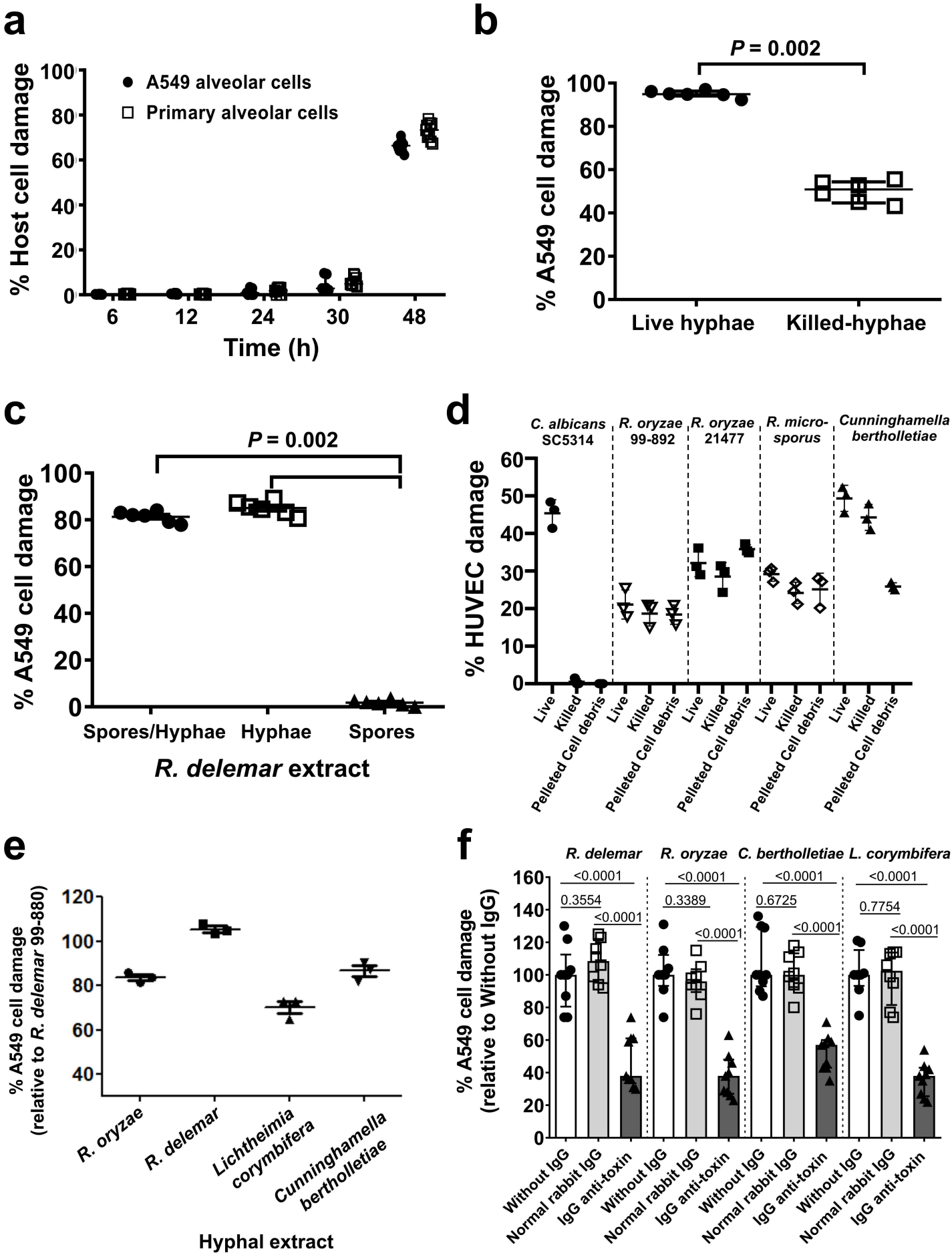

Extended Data Figure 2

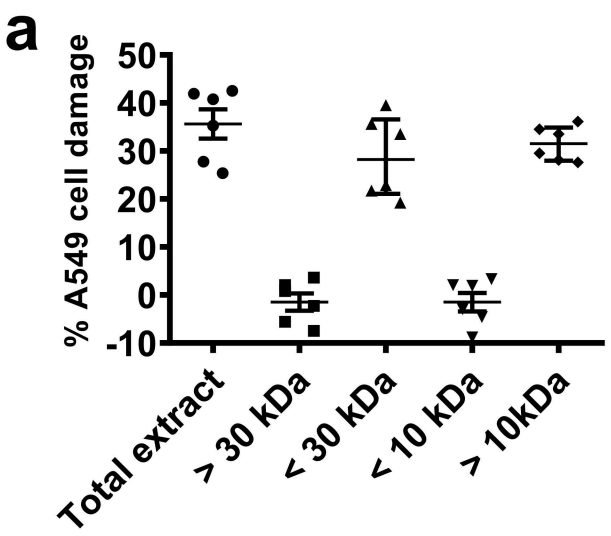

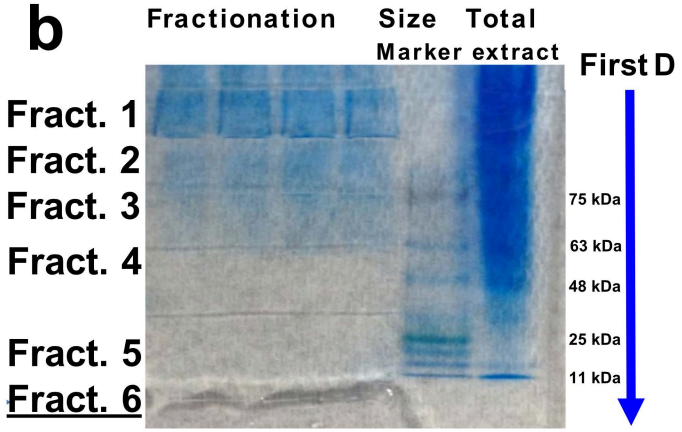

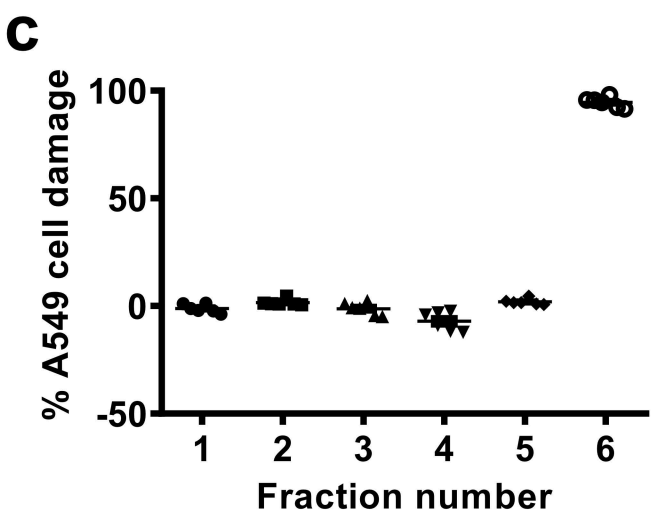

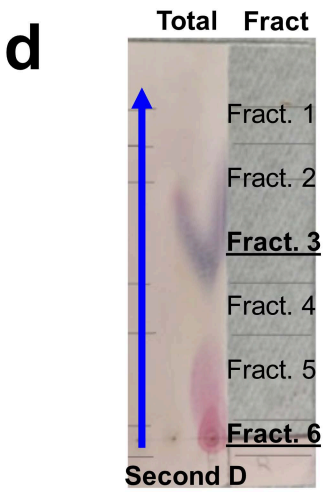

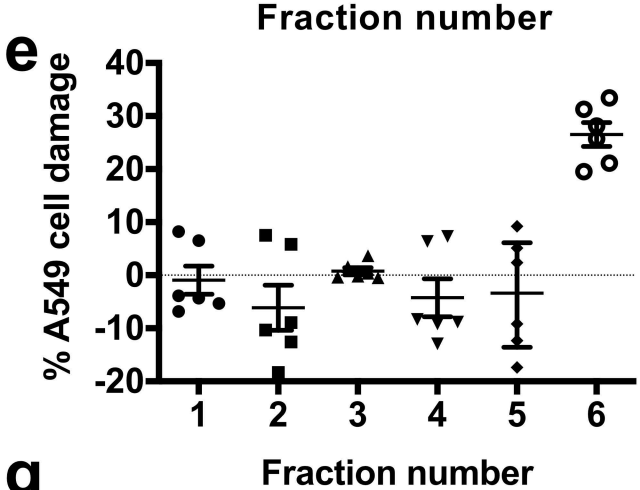

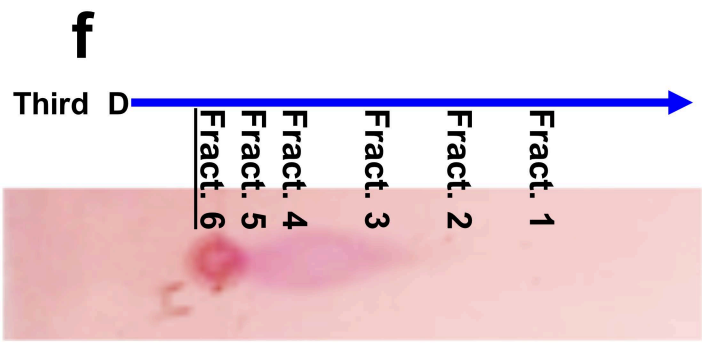

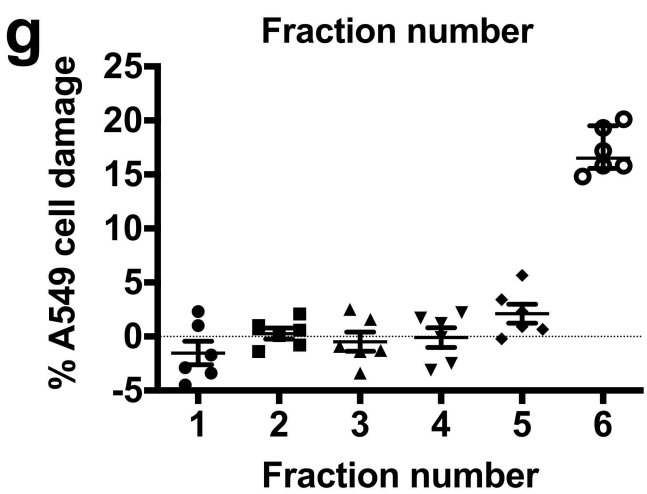

Extended Data Figure 3

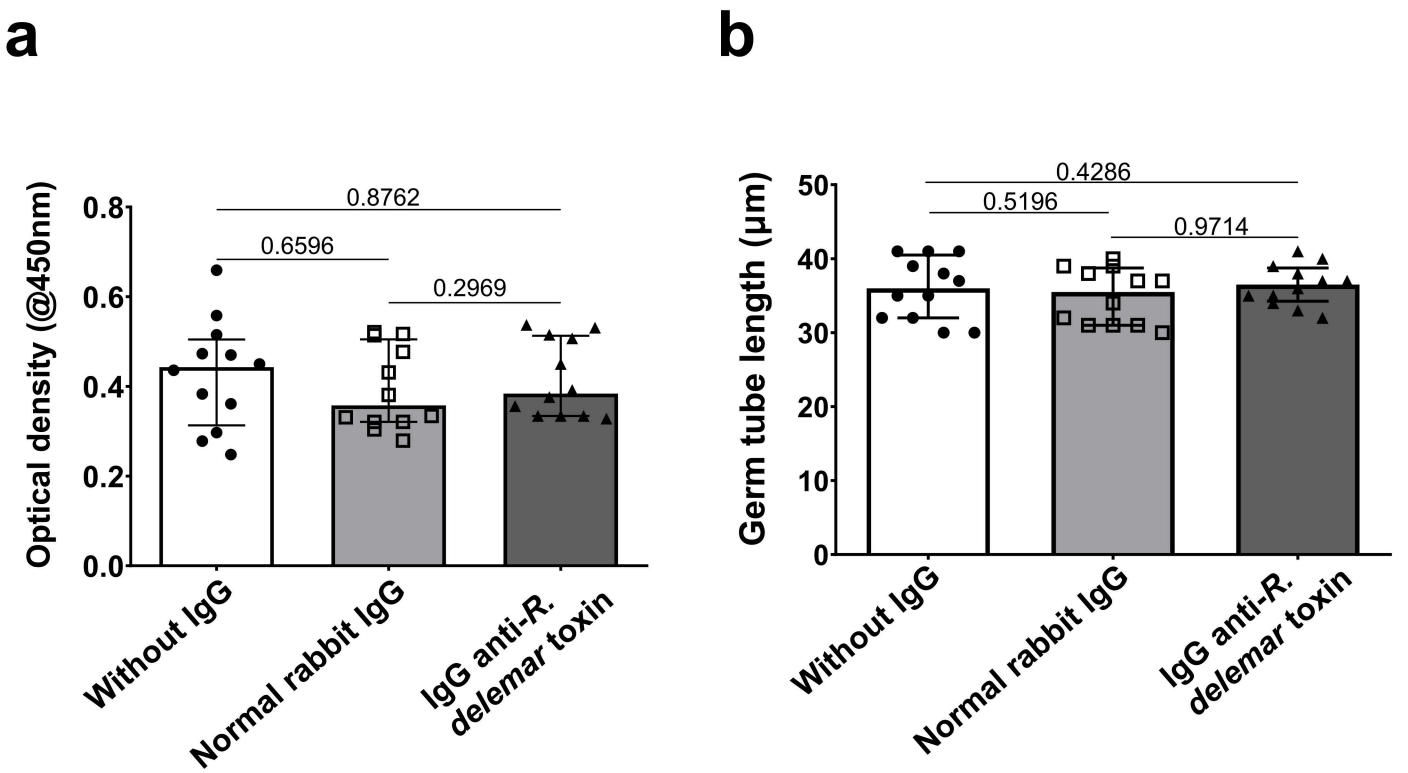

Extended Data Figure 4

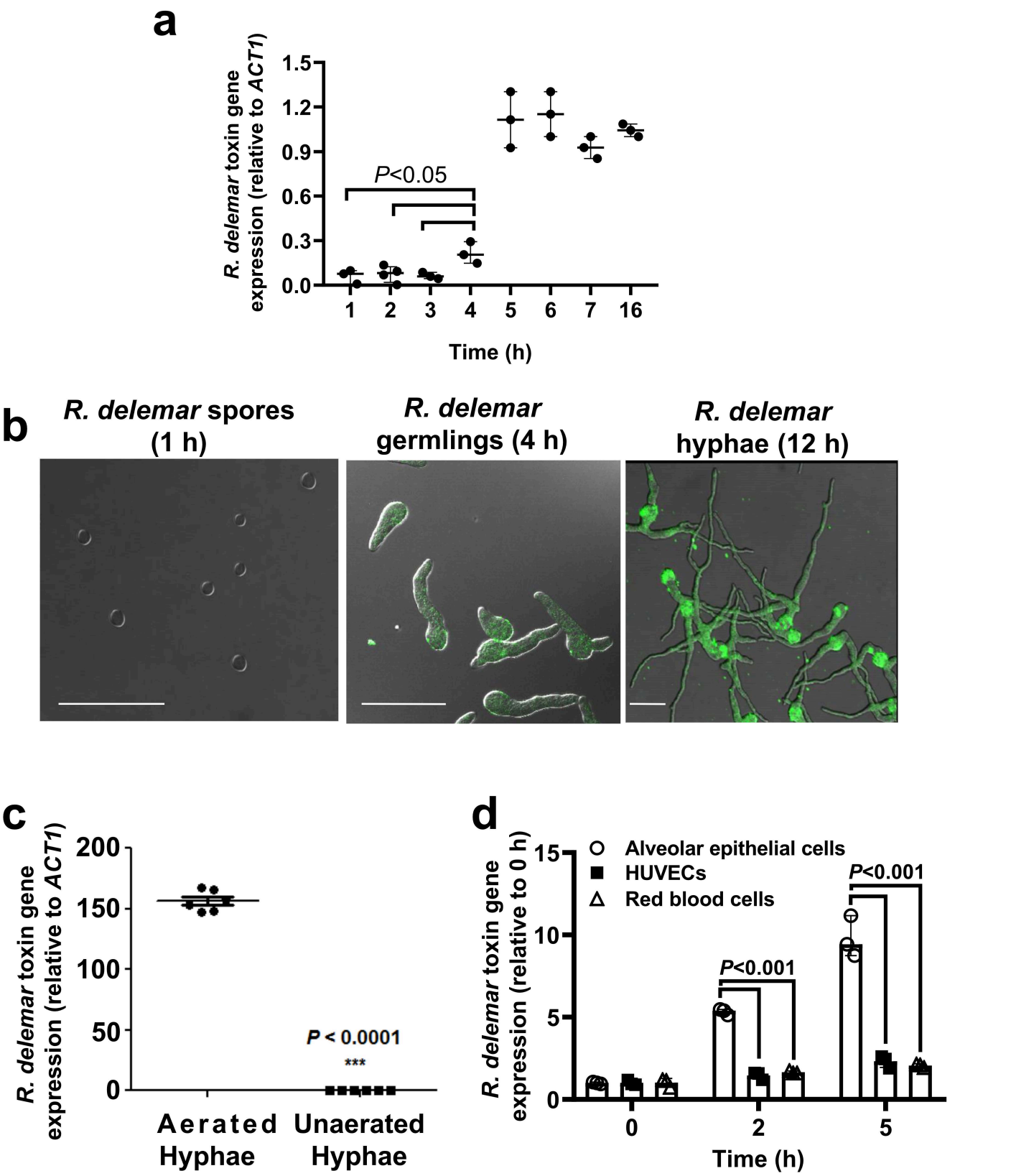

Extended Data Figure 5

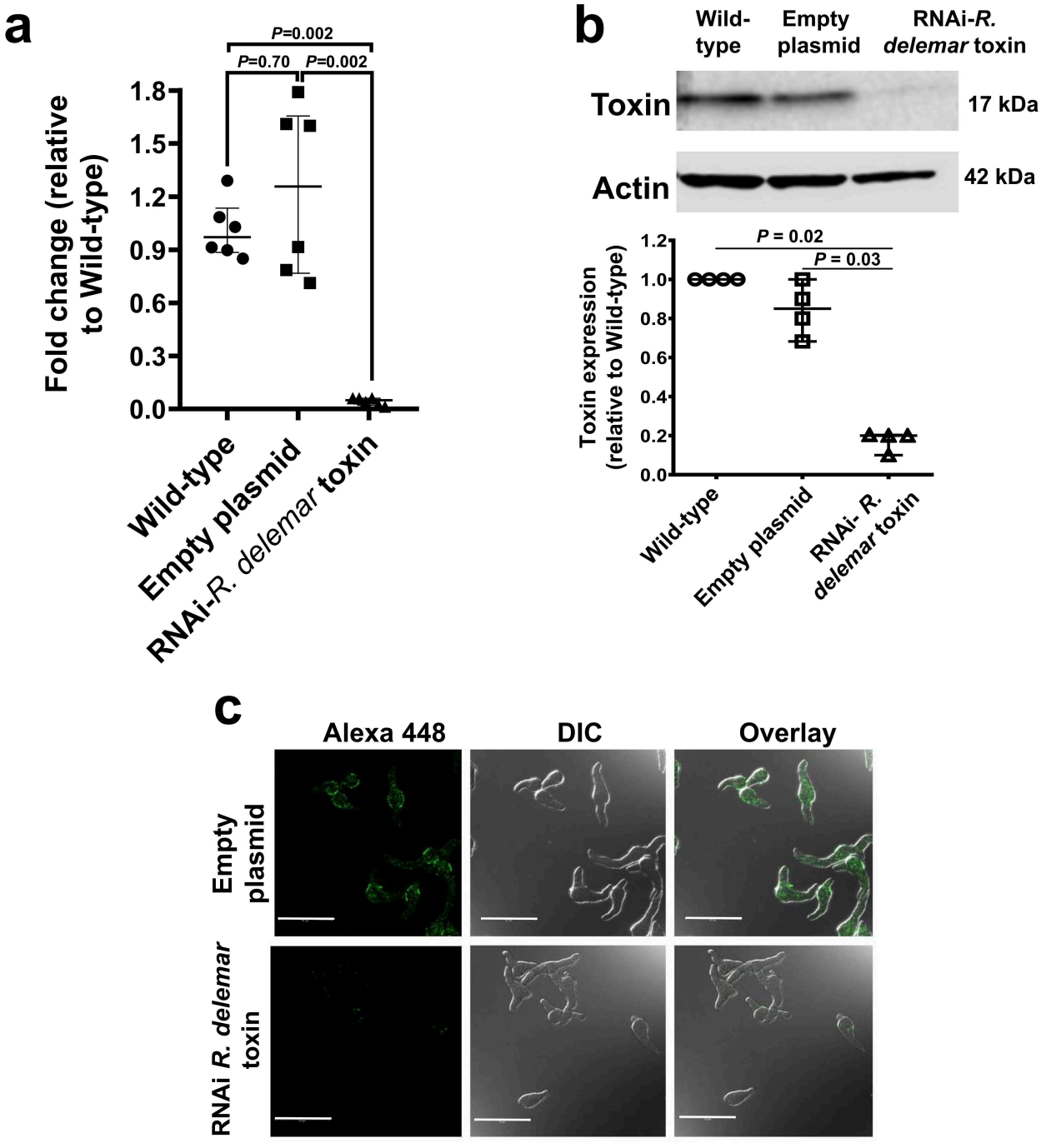

Extended Data Figure 6.

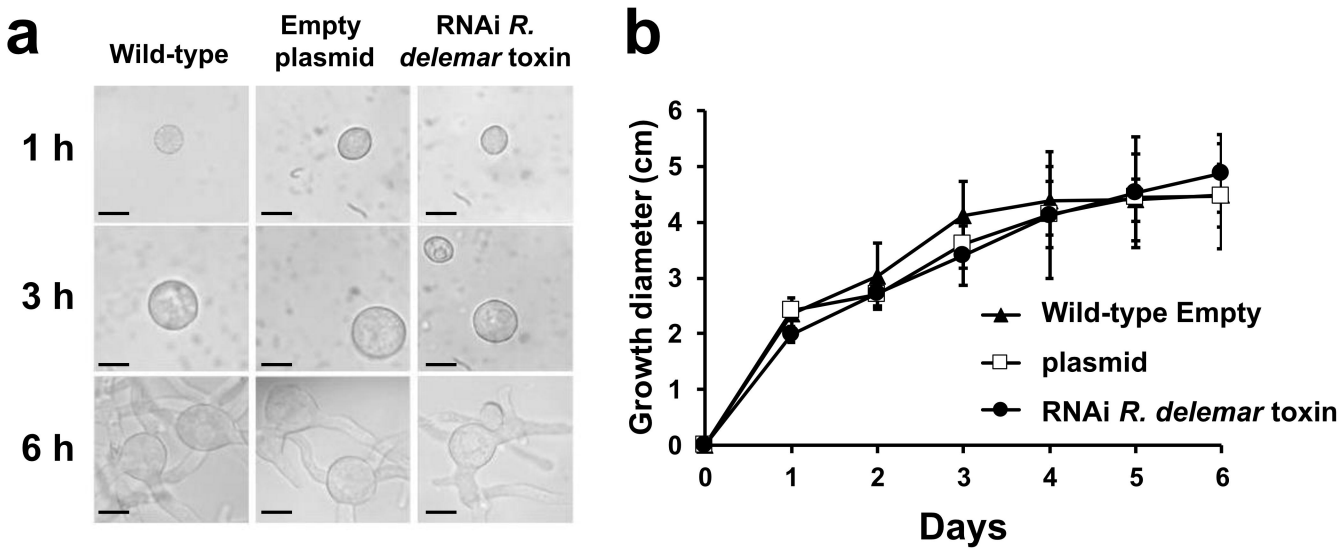

Extended Data Figure 7.

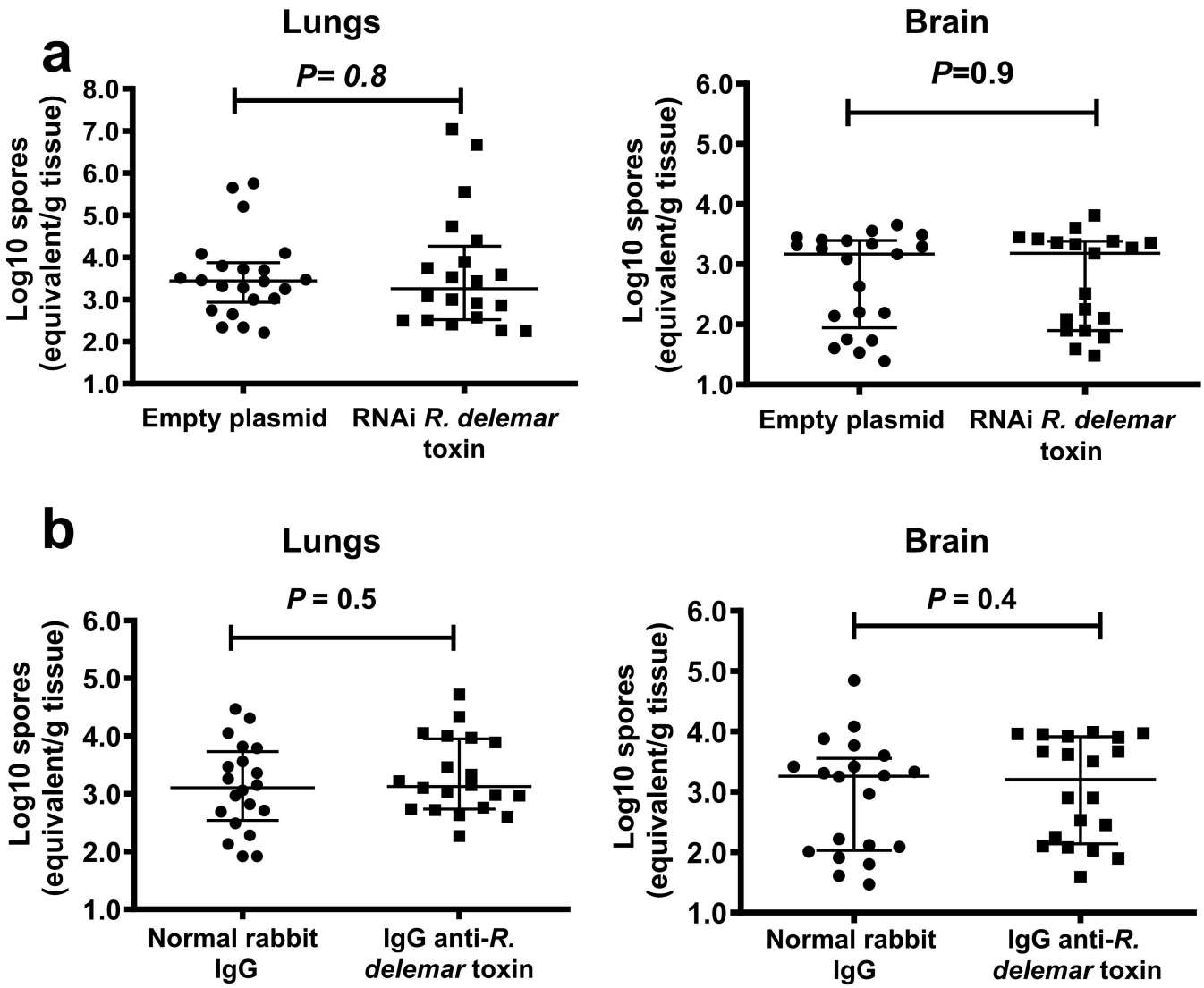

Extended Data Figure 8

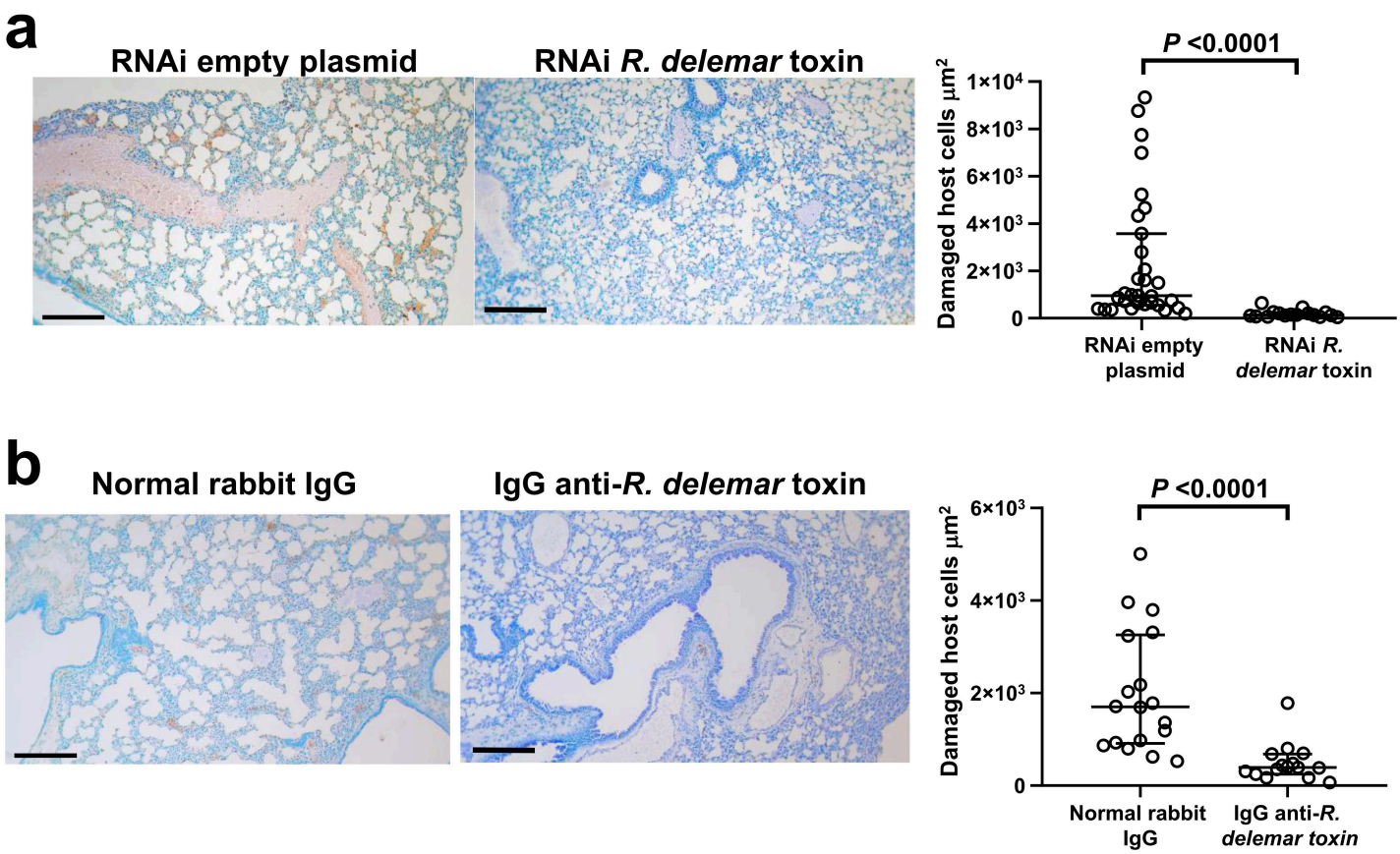

Extended Data Figure 9

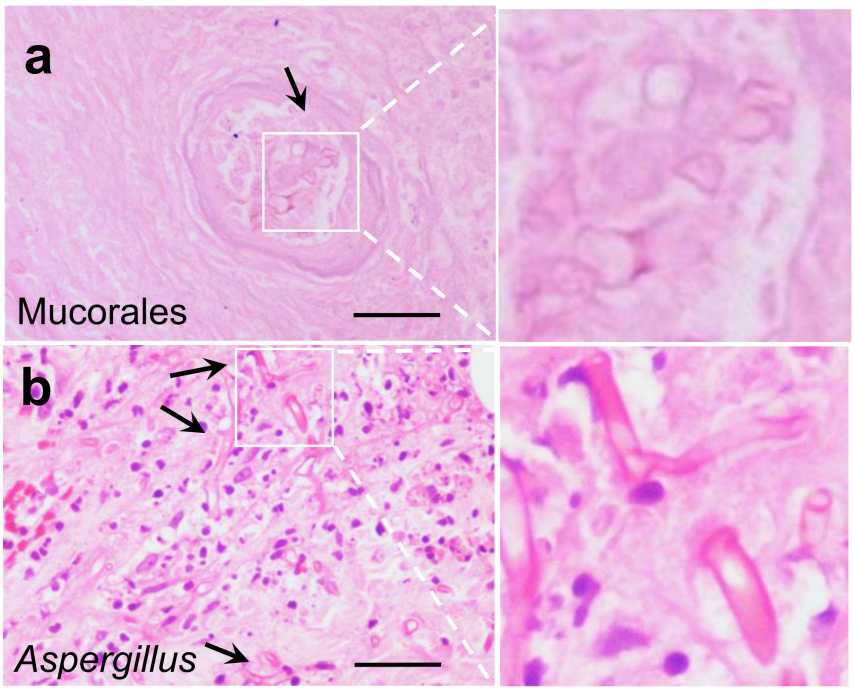

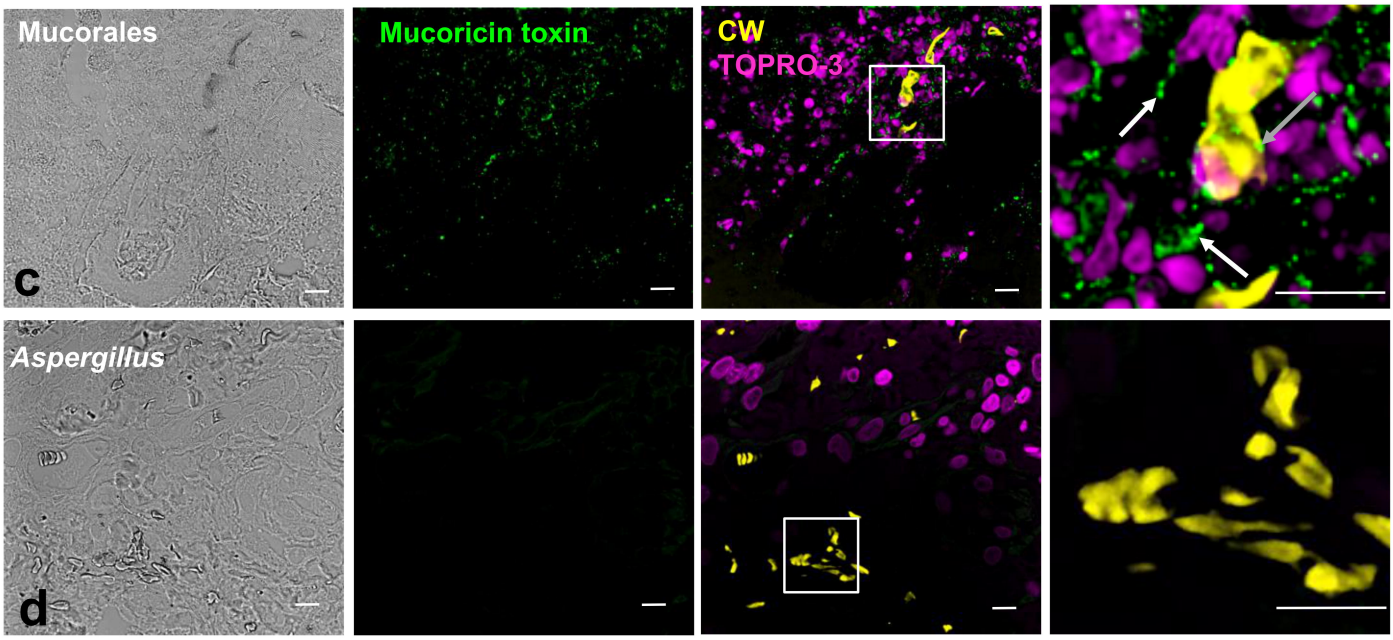

Extended Data Figure 10